https://doi.org/10.3311/PPch.41572

Periodica Polytechnica Chemical Engineering, 69(4), pp. 697–719, 2025

A Hybrid Deep Learning and Statistical Approach for Fault Detection and Diagnosis in AGRU Systems: Integration with Aspen Plus and Explainable AI

Nadia Khan[1], Syed Ali Ammar Taqvi[2*], Maria Waqas[3]

[1] Department of Polymer and Petrochemical Engineering, Faculty of Chemical and Process Engineering, NED University of Engineering and Technology, University Road, 75270 Karachi, Pakistan
[2] Department of Chemical Engineering, Faculty of Chemical and Process Engineering, NED University of Engineering and Technology, University Road, 75270 Karachi, Pakistan
[3] Department of Computer and Information Systems Engineering, Faculty of Electrical and Computer Engineering, NED University of Engineering and Technology, University Road, 75270 Karachi, Pakistan
* Corresponding author, e-mail: aliammar@neduet.edu.pk

Received: 10 July 20255, Accepted: 03 October 2025, Published online: 30 October 2025

Abstract

Fault detection and diagnosis are vital functions in process industries, supporting real-time monitoring and ensuring plant safety. However, the presence of complex, high-dimensional, and highly correlated process data presents a significant challenge for traditional monitoring systems. In natural gas processing, the acid gas removal unit is a critical subsystem responsible for removing acid gases such as hydrogen sulfide and carbon dioxide. Faults such as foaming, tray corrosion, cooler fouling, low gas flow, and reduced amine circulation are common in AGRUs but have received limited attention in the literature, highlighting a significant research gap. To address this, a comprehensive study was conducted by simulating the AGRU process and its associated faults using Aspen Plus Dynamics. This enabled the generation of realistic, multivariate time-series data under normal and faulty operating conditions. For the fault detection phase, two approaches were developed and comparatively evaluated: principal component analysis, which employs Hotelling's T^2 and squared prediction error metrics, and a long short-term memory autoencoder, which utilizes reconstruction error and leverages sequential learning. Subsequently, a fault diagnosis was performed using bidirectional recurrent neural networks, specifically Bi-GRU and Bi-LSTM models, which were trained to classify fault types based on their temporal signatures. The Bi-GRU model demonstrated superior performance with an accuracy of 99.8% and an F1-score of 99.6%, indicating its suitability for robust fault classification. To enhance model interpretability, shapley additive explanations were applied to identify critical input variables influencing model predictions, and the results were compared with those from local interpretable model-agnostic explanations.

Keywords

acid gas removal units, fault detection and diagnosis, deep learning, principal component analysis (PCA), gated recurrent unit (GRU), long short-term memory (LSTM)

1 Introduction

Process safety and risk management remain critical challenges in the process and manufacturing industries. To enhance safety, digital systems are increasingly integrated across the entire lifecycle of process plants, driven by the advancements of Industry 4.0, which promotes automation, digitalization, and intelligent operations [1]. While distributed control systems (DCS) and advanced process control (APC) have improved process monitoring and control, managing abnormal operating conditions still heavily relies on manual intervention contributing to approximately 70% of production accidents. In process industries, there is a growing demand for high product quality, minimal operational downtime, and enhanced safety [1–3]. However, human error remains a predominant factor, accounting for approximately 70% of industrial accidents, which in turn leads to substantial economic losses and environmental impacts [4–6]. Despite advancements in control systems, catastrophic incidents have occurred, such as the Bhopal disaster in India and the Mina Al Ahmadi Refinery explosion in Kuwait, which

Cite this article as: Khan, N., Taqvi, S. A. A., Waqas, M. "A Hybrid Deep Learning and Statistical Approach for Fault Detection and Diagnosis in AGRU Systems: Integration with Aspen Plus and Explainable AI", Periodica Polytechnica Chemical Engineering, 69(4), pp. 697–719, 2025. https://doi.org/10.3311/PPch.41572

resulted in significant fatalities and financial losses. Additionally, minor industrial incidents occur daily, resulting in billions of dollars in annual losses due to unsafe operations [7]. Fault detection (FD) is crucial for ensuring system safety and facilitating practical risk assessment. It enables the identification of abnormalities, preventing minor issues from escalating into major failures. Enhancing operational safety and reliability, it helps mitigate risks, supports predictive maintenance, and improves decision-making. FD also ensures compliance with safety regulations and contributes to efficient and cost-effective system performance [8].

Research in fault detection and diagnosis (FDD) has seen significant advancements, driven by the adoption of advanced methodologies, including deep learning, big data analytics, and hybrid or multimodal approaches [9–12]. Data-driven approaches, including statistical and machine learning techniques, are increasingly being employed to enhance FD in industrial systems. Principal component analysis (PCA) remains a popular method due to its simplicity and effectiveness [13]. To overcome the limitations of individual methods, hybrid approaches have been developed that combine multiple techniques to enhance diagnostic performance [14]. Notably, Copula-Bayesian models and strong relevant mechanism Bayesian networks (SRMBN) have demonstrated promise in risk modeling and fault diagnosis [15]. However, traditional models often struggle with feature extraction from high-dimensional data, underscoring the need for more scalable solutions. In this context, Alauddin et al. [16] proposed a robust artificial neural network (ANN) model that addresses issues of mislabeled and low-quality data by integrating data quality features derived from Mahalanobis distance, outperforming conventional ANNs under higher mislabeling levels. Similarly, an early FD method in forced-oxidation systems was developed using an attention-based long short-term memory (LSTM) network for predictive maintenance [17]. Additionally, Tao et al. [18] introduced a triage-based convolutional neural network (Tr CNN) for fault diagnosis in the Tennessee Eastman (TE) process, which overcame the limitations of single-model strategies by adapting models to specific fault types, thereby improving diagnostic accuracy. Collectively, these advancements contribute to more precise and efficient FD across a range of industrial applications.

Natural gas is considered a cleaner energy source; however, impurities such as H_2S and CO_2 must be removed to prevent environmental harm. Amine-based absorption in acid gas removal units (AGRUs) remains the most efficient method for this purpose [19–22]. Ensuring AGRU's efficient and safe operation reduces emissions, supports global climate goals, and aligns with the sustainable development goals (SDGs) for clean energy and climate action. Advances in purification technology further enhance sustainability and energy security [3, 23–25].

As a multivariate and complex process, monitoring of AGRUs is crucial for accurately measuring the composition of acid gases [26, 27]. Various sensors are employed to monitor the critical variables of the unit [28]. The performance of AGRUs is often affected by common issues, including disturbances in cooler duty, fouling and deposition of contaminants or heat-stable salts (HSS), reduced tray efficiency, and fluctuations in feed composition and temperature [29, 30]. These faults can adversely impact the purity of natural gas as well as the temperature and pressure profiles within the absorption column. To prevent performance decline caused by faulty systems, developing robust FD methods is crucial for improving operational safety, efficiency, and ensuring uninterrupted production. Furthermore, optimizing AGRU operations supports the energy sector's broader objective of balancing global energy demands with environmental sustainability [31–33].

In previous studies, the monitoring of AGRU has been carried out by a large variety of shallow learning models, which mark the early stage of machine learning evolution [34–36]. Pradittiamphon and Wongsa [37] demonstrated the partial least squares (PLS) capability of FD in the gas absorption process, helping to prevent costly interventions. In another study, Hakimi et al. [22] utilized ANN to effectively detect faults in a CO_2 scrubbing column using data generated from Aspen Plus. In a different approach, Al-Sinbol and Perhinschi [38] employed artificial immune systems, which were validated using a rigorous dynamic model of the gas absorption unit. This method successfully identified 14 abnormal conditions, such as accumulated salts and leaks, within the system [38]. The mentioned literature shows that various models have been developed for FD in chemical processes, but the root cause identification in AGRUs using deep learning remains scarce [39–43].

Deep learning has emerged as a transformative technology for fault diagnosis and process optimization in the chemical and pharmaceutical industries, providing innovative solutions to several challenges faced in traditional methods [44–47]. By leveraging multiple layers

of nonlinear processing units, deep learning networks can effectively model complex processes, automatically extract features from raw signals, and improve predictive accuracy [48, 49]. Unlike shallow learning, deep learning offers a superior network structure, enhancing its ability to handle intricate tasks [31, 50].

Recent research has explored deep learning models for FDD in chemical processes [51–53]. Deep learning approaches have demonstrated promising results in FDD for chemical processes, particularly in improving the accuracy and efficiency of detecting incipient faults [54]. A deep learning-based FDD model utilizes gated recurrent units (GRUs) and LSTM networks to analyze time-series sensor data. These architectures incorporate gating mechanisms to effectively capture temporal dependencies, enabling the differentiation between normal and faulty operating conditions. This makes them particularly suitable for modeling complex and nonlinear chemical processes [55, 56]. Various deep learning architectures have been explored, including deep autoencoders [57], stacked sparse autoencoders [54], extended deep belief networks [55], and dense feed-forward neural networks [52]. These methods demonstrated improved accuracy in fault classification and early detection compared to traditional statistical techniques [52]. These models were successfully applied to benchmark datasets such as the TE process [54, 56] and real-world applications, including natural gas pumping units [52].

Deep convolutional neural networks (DCNNs) have demonstrated excellent performance in diagnosing faults in the TE process benchmark [51]. In addition, LSTM recurrent neural networks (RNNs) have outperformed traditional FDD methods in learning long-term patterns [51, 58]. Hybrid models that integrate convolutional networks, LSTM, and attention mechanisms demonstrated promising results in capturing spatial and temporal features, achieving superior accuracy in fault diagnosis [59]. Deep learning models excel in FDD due to their ability to automatically extract meaningful features from raw sensor data and effectively capture the dynamic behavior of industrial processes [60]. Despite significant advancements in deep learning for chemical process monitoring, critical research gaps persist in its application to AGRUs.

To address existing gaps in FDD for safety-critical processes such as AGRUs, this study presents a novel, structured, and interpretable deep learning-based framework tailored for multivariate time-series process data. The novelty of this work lies in its integration of sequential deep learning models with explainable AI techniques that enhance both performance and interpretability in FDD.

The proposed methodology follows a systematic three-phase structure:

1. FD using long short-term memory autoencoders (LSTM-AEs) compared with traditional PCA,
2. fault classification through bidirectional gated recurrent units (Bi-GRUs) and bidirectional long short-term memory (Bi-LSTM) networks, and
3. model interpretability via shapley additive explanations (SHAP).

Comparative analysis in phase one highlights the trade-offs between statistical and deep learning methods in identifying anomalies. Phase two leverages the temporal learning capabilities of bidirectional architectures to improve classification accuracy and support robust root cause analysis. Finally, phase three introduces SHAP to overcome the "black-box" limitations of deep models by providing feature-level attributions that are transparent and actionable for process engineers.

The main contributions of this study are threefold:

- A comparative performance assessment between conventional PCA and LSTM-AE for anomaly detection in multivariate time-series data.
- The deployment of Bi-GRU and Bi-LSTM models to enhance fault diagnosis by capturing bidirectional temporal dependencies.
- The application of SHAP for interpretability enables domain experts to understand and trust model predictions in complex process environments.

2 Multi-class fault detection and diagnosis algorithm

The hybrid model presented in this study focuses on FD in the AGRU system, utilizing both LSTM-AE and PCA-based methods to evaluate their effectiveness. Bi-LSTM and Bi-GRU models were employed to accurately diagnose faults by capturing temporal dependencies within the process data. This approach enables real-time deployment on edge devices such as programmable logic controllers (PLCs) and DCS, which are commonly used in industrial AGRU operations. The integration of these techniques provides a robust framework for FDD, as illustrated in Fig. 1.

The methodology comprises several structured steps. First, time-series data representing normal and abnormal operating conditions were generated using Aspen Plus Dynamics. Six process faults were simulated under a closed-loop configuration, monitoring the response of 18 variables. Each fault was introduced after 10 h of normal operation, resulting in seven distinct faults (one normal and six fault conditions). The generated dataset was

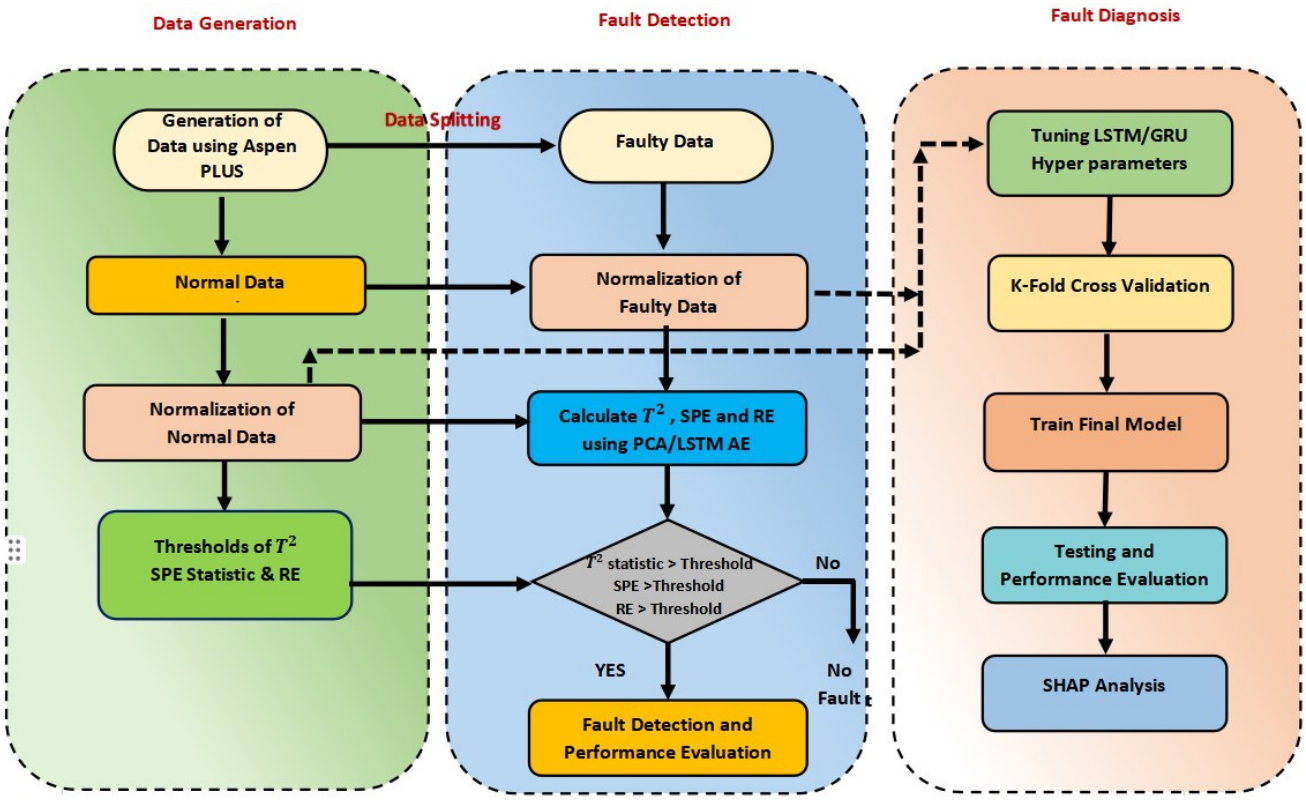

Fig. 1 Flowchart of DL algorithm for FDD

structured as a matrix of dimensions [4600 × 7 × 18]. In the second step, the dataset was split into 18 features and 7 fault labels. The third step involved handling missing values, detecting outliers, and normalizing the data. In the fourth step, PCA/LSTM-AE were applied to transform the data and calculate statistical metrics, including Hotelling's T^2 statistic, squared prediction error (SPE), and reconstruction error (RE). The fifth and sixth steps involved parameter tuning and *K*-fold cross-validation to optimize model performance. In the seventh and eighth steps, the processed data was used to train an optimized deep learning model for root cause analysis. The ninth and tenth steps focused on testing the model and evaluating its diagnostic performance. Finally, the eleventh step addressed the interpretability of deep learning outputs using SHAP and local interpretable model-agnostic explanations (LIME).

In the Supplement, Algorithm S1 summarizes the complete methodology adopted for developing the proposed PCA–deep learning-based fault analysis framework.

3 Data generation using Aspen Plus

3.1 Process description

AGRU employs amine-based solvents to eliminate unwanted CO_2 from natural gas, making it suitable for domestic and commercial applications [3]. The amine-based gas-sweetening process involves three primary columns. In the absorption column, acid gases are removed from natural gas through a reaction with the amine solution, resulting in a rich amine stream exiting the column. This rich stream is then directed to the second column, where it undergoes flashing before being sent to the stripper. In the stripper, the amine is regenerated by separating the absorbed acid gases from the solution. The regenerated amine is subsequently recycled back to the absorption column for reuse.

In this study, the flow rates, temperature, pressure, and composition of the sour gas were defined based on data from the gas field, as shown in Table 1. A steady-state

Table 1 Process parameters for AGRU process

Parameter*	Value	Parameter	Value
Molar flow rate (kmol/h)	5680	n-C_5	0.03%
Temperature (°C)	35	Nitrogen	7.49%
Pressure (bar)	57	CO_2	4.6%
C_1	85.39%	MDEA	50 wt%
C_2	1.36%	Pressure (bar)	54
C_3	0.55%	Temperature (°C)	43
i-C_4	0.16%	No of trays	20
n-C_4	0.13%	Tray spacing (m)	0.69
i-C_5	0.05%		

* C_1 is methane, C_2 is ethane, C_3 is propane, C_4 is butane, C_5 is pentane.

simulation was developed using Aspen Plus V10.0 [61], employing the electrolyte non-random two-liquid (eNRTL) thermodynamic model with an equilibrium-based approach. The primary CO_2 recovery unit in the simulation was a RadFrac absorption column. The sour gas entered the column at 57 bar and 35 °C, while a 50 wt% methyldiethanolamine (MDEA) solution was introduced at 54 bar and 45 °C. The column consisted of 20 trays with a tray spacing of 0.69 m, meeting the criteria for satisfactory separation performance. The amine feed was introduced at tray 2, and the sour gas entered at tray 19. To ensure the sweet gas stream contained less than 2 mol% CO_2, an acid gas-to-amine ratio of 0.35 mol acid gas per mol amine was maintained, in compliance with environmental regulations [19].

The steady-state simulation results were validated against actual operating conditions from the gas field. Key parameters included a top-column CO_2 composition of less than 2 mol%, an acid gas-to-amine loading of 0.35, a column top pressure of 54 bar, rich amine pressure of 55.5 bar, regenerator operating pressure of 2.1 bar, and a reboiler bottom temperature of 131 °C. For the development of the dynamic simulation, the regenerator pressure was slightly increased to 2.2 bar to ensure convergence, accounting for additional inlet/outlet valves and the corresponding pressure drop across each tray. Once the steady-state simulation was successfully converged, it was exported to Aspen Plus Dynamics V10.0 [61] in pressure-driven mode, as shown in Fig. 2. As Aspen Plus Dynamics does not support rate-based models, an equilibrium model was used instead. To mitigate deviations from rate-based behavior, vaporization efficiency was considered in the steady-state configuration. Design specifications for valves, coolers, heaters, and the absorption column were defined to ensure stable dynamic operation. Since controller configuration and tuning are critical in dynamic simulations, multiple control strategies were implemented. Pressure, level, concentration, and flow controllers were successfully configured. Controller gains (*Kc*) were determined individually for each controller, and tuning was carried out using the Ziegler–Nichols method. All controllers were modeled in automatic mode. Specifically, pressure, concentration, and level controllers were set to direct-acting mode, while flow and temperature controllers were configured in reverse-acting mode.

4 Process faults

The Aspen Plus dynamic simulation of the AGRU, as described earlier, was used to generate both normal and faulty datasets. Faults were introduced as disturbances that caused deviations from normal operating conditions. The plant was operated under fault-free conditions for 40 h to capture baseline data, during which all process variables remained within their specified operating ranges. To simulate fault conditions, a total of six distinct faults were introduced into the AGRU simulation, as summarized in Table 2. Each fault scenario was initiated after 10 h of normal operation and comprised 1,000 normal samples followed by 3,600 faulty samples. The deviations in the behavior were observed in 18 process variables, as shown in Table 3. White noise was added to the clean data obtained from Aspen Dynamics using Eq. (1) to simulate sensor noise, mimicking sensor inaccuracies typically observed in field instruments. The noise was modeled based on standard deviations representing 1–5% of the typical signal range for each sensor. This approach helps test the model's tolerance to mild-to-moderate disturbances and evaluate generalization under varying signal-to-noise

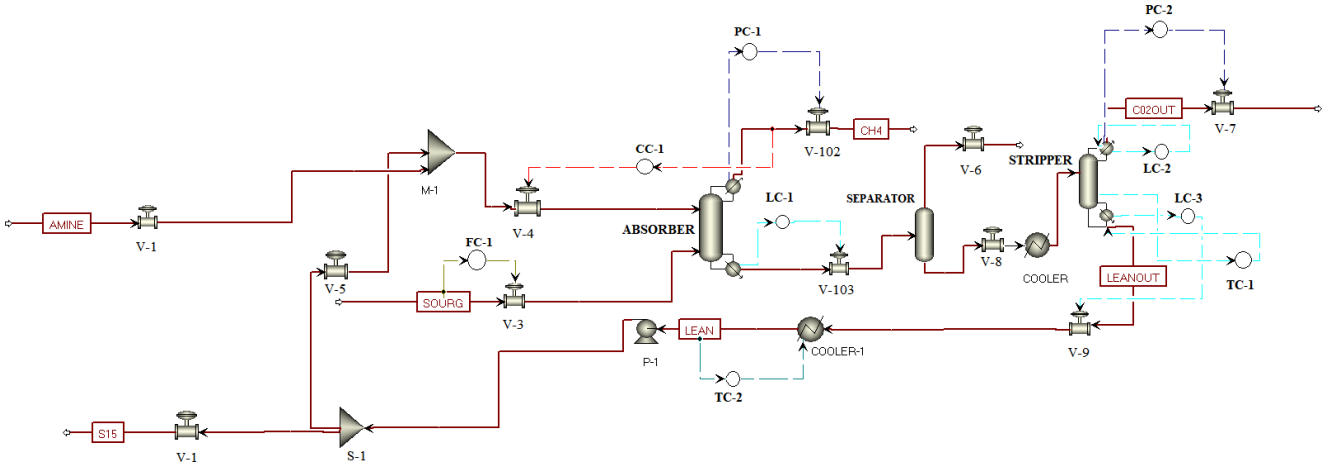

Fig. 2 Process flow diagram of AGRU

Table 2 AGRU fault descriptions

Fault	Abbreviation	Fault	Abbreviation
Normal condition	N	Increase in differential pressure	F_4
Cooler fouling	F_1	Loss of amine flow	F_5
High sour gas temperature	F_2	Damaged tray	F_6
High gas flow	F_3		

Table 3 Measured process variables of AGRU

Parameter	Abbreviation	Parameter	Abbreviation
Sour gas pressure (bar)	x_1	Rich amine pressure (bar)	x_{10}
Sour gas temperature (°C)	x_2	Rich amine temperature (°C)	x_{11}
Sour gas flowrate (kmol/h)	x_3	Rich amine flow (kmol/h)	x_{12}
Amine temperature (°C)	x_4	Tray 1 liquid level (m)	x_{13}
Amine flow (kmol/h)	x_5	Tray 4 liquid level (m)	x_{14}
CO_2 composition in sweet gas (°C)	x_6	Tray 10 liquid level (m)	x_{15}
Sweet gas pressure (bar)	x_7	Tray 14 liquid level (m)	x_{16}
Sweet gas temperature (°C)	x_8	Tray 19 liquid level (m)	x_{17}
Sweet gas flow (kmol/h)	x_9	Bottom level (m)	x_{18}

ratios. Although synthetic sensor noise is introduced into the dataset to mimic real-world conditions, it may not fully represent the complex and dynamic nature of sensor disturbances typically observed in industrial AGRU environments. Real-world noise can vary significantly across different operating regimes, potentially obscuring subtle fault signatures and affecting the reliability of model predictions. Additionally, the presence of noise may lead to misleading rankings of feature importance, thereby reducing the model's interpretability. These limitations could compromise FD accuracy, particularly during transitional phases or abnormal operating conditions. To address these limitations, future work will focus on enhancing the model's real-world applicability by incorporating actual sensor datasets from operating AGRUs, including historical fault events and maintenance records. This will enable benchmarking of the current model's performance under real plant conditions. Additionally, techniques such as transfer learning and online fine-tuning will be explored to adapt the model to plant-specific noise patterns and operational variations. To further enhance noise resilience, domain-specific filtering methods, such as Kalman filters or wavelet-based denoising, will be integrated during the preprocessing stage, ensuring more robust and accurate FD in practical deployment scenarios.

$$X_{\text{noisy}} = X_{\text{clean}} + N\left(0, \sigma^2\right) \tag{1}$$

Following standard deep learning practices, the collected dataset was divided into 70% training, 15% validation, and 15% test sets, which is a widely used approach in machine learning, particularly for medium-sized datasets, as detailed in Table 4. The primary reason for this allocation is to ensure that the model has enough data to learn effectively while still maintaining reliable validation and testing sets. The training set, which comprises the largest portion (70%), enables the model to capture the underlying patterns and relationships in the data. Meanwhile, the validation set (15%) serves as an intermediary checkpoint, helping to fine-tune hyperparameters, select the best model, and detect overfitting during the development phase. The test set (the remaining 15%) acts as an unbiased evaluation of the final model's performance, ensuring that the results reflect how well the model generalizes to unseen data.

A detailed description of each fault is provided below.

4.1 Fault 1: cooler fouling

Maintaining precise control over the amine temperature is critical to meeting the required CO_2 specifications. The amine cooler's duty decreases over time due to corrosion and fouling, which are primarily caused by the deposition of heat-stable amine salts, degradation products, and amino acids. This reduction in cooler duty significantly impacts the amine temperature [29]. The first fault (F_1) was introduced by decreasing the cooler duty, which directly affected the amine temperature. As the temperature rises,

Table 4 Parameter specifications for data acquisition

Parameter	Value
Sampling interval	0.01 h
Total number of samples/faults	4600
Normal samples in each fault	1000
Faulty samples in each fault	3600
Training set size	70%
Validation set size	15%
Test set size	15%
White noise (band-limited white noise)	x = 0.0003, Pressure = 0.0002

the viscosity of the amine decreases, potentially leading to foaming on the tray. Additionally, excessively high temperatures can reduce the physical solubility of CO_2 in the MDEA solution [62, 63].

4.2 Fault 2: high sour gas temperature

The second fault (F_2) corresponds to an increase in temperature of the sour gas entering the system. Malfunctioning gas coolers, air preheaters, or heat exchangers can result in insufficient cooling before absorption. Additionally, excessive gas compression, such as from improper compressor settings, can lead to a temperature rise due to adiabatic heating, disrupting the overall temperature profile of the column. The reaction between CO_2 and MDEA is exothermic; therefore, an increase in column temperature reduces the driving force for mass transfer, thereby decreasing the absorption rate. For this reason, monitoring and controlling the amine temperature is essential to keep it within the optimal range. Proper temperature regulation helps prevent foaming when processing gas and other hydrocarbon sources. Sour gas can undergo hydrocarbon condensation below 25 °C, while the CO_2 concentration in the amine rises significantly above 45 °C [21]. To achieve optimal performance, the gas temperature should be maintained between 25–35 °C, and the amine temperature should be kept within 40–45 °C. Increasing the gas temperature can gradually reduce the CO_2 recovery efficiency [27].

4.3 Fault 3: high gas flow

By considering the reservoir conditions, the third fault (F_3) is associated with an elevated sour gas flow rate. This typically happens due to higher production rates from the upstream wells or process units, leading to a higher flow rate of untreated (sour) gas. This is common when new wells are brought online or when production conditions change. Moreover, if the inlet gas compression system is not working efficiently, the volume of gas entering the system may increase due to pressure variations. Additionally, malfunctioning of the inlet control valve may allow excessive sour gas to enter the contactor, leading to higher flow rates. This increase in sour gas flow may also cause flooding in the column. Flooding is a hydrodynamic phenomenon where a portion of the liquid phase is carried to the tray above, causing droplet ejection from the froth due to an increased gas rate [64]. This liquid accumulation leads to column flooding, significantly reducing separation efficiency and capacity [65, 66]. Flooding is typically identified by a sharp rise in tray differential pressure, increased column pressure drops, and a loss of separation performance [27].

4.4 Fault 4: increase in differential pressure

The fourth fault (F_4) is related to increased pressure drop in the column, reflecting a foaming scenario. Foaming is a common issue in absorbers that can impact CO_2 recovery. It typically occurs when foam-promoting contaminants enter the plant with the feed. Foam formation and stability are influenced more by the surface properties of the liquid phase than by physical factors like temperature and pressure. A foaming amine plant is identified by high and erratic differential pressure in the absorber column [65], along with fluctuating levels, amine carryover to downstream systems, and reduced production capacity [57].

4.5 Fault 5: loss of amine flow

The fifth fault (F_5) is triggered by the reduction in the amine flow, which badly affects the CO_2 separation efficiency. Several factors can cause this issue such as valve sticking and pump malfunctioning [64]. Due to the reduction in amine flow, the gas-to-liquid ratio increases, reducing mass transfer efficiency. Poor circulation may also cause fluctuating gas pressures in the column [65].

4.6 Fault 6: damaged tray

The sixth fault (F_6) is related to a reduction in tray efficiency in the absorption column, indicating possible corrosion caused by solvent degradation. Solvent degradation represents a critical operational challenge in amine-based absorption systems, primarily due to the formation of HSS and corrosive by-products. These undesirable contaminants in solvents tend to be abrasive to the protective layer of the tray, causing corrosion on the tray. These degradation mechanisms contribute to accelerated corrosion rates, particularly affecting the absorber and stripper trays, which subsequently diminishes tray efficiency and compromises mass transfer performance. To systematically evaluate the repercussions of solvent degradation within the proposed fault diagnosis framework, this phenomenon has been incorporated as reduced tray efficiency. This fault condition emulates the long-term cascading effects of solvent degradation, including impaired CO_2 absorption capacity, elevated reboiler energy demand due to inefficient separation, and potential operational instabilities. The selection of reduced tray efficiency as a representative fault is motivated by its ability to encapsulate the multifaceted impact of solvent degradation while enabling

measurable deviations in critical process parameters, such as CO_2 loading, lean amine purity, reboiler duty, and column pressure drop. By integrating this fault scenario, the proposed model is rigorously validated against both common operational disturbances and severe degradation-induced failures, ensuring robustness in real-world industrial applications [29, 67].

5 Model development for fault detection and diagnosis

5.1 Fault detection

Section 5.1 outlines the implementation of the proposed FD algorithms. Various anomaly detection techniques have been explored in the literature to address this complexity [68, 69]. In this study, two approaches LSTM-AE and PCA—were employed for fault identification in an AGRU. The performance of the LSTM-AE model was compared with that of PCA-based detection techniques, specifically using Hotelling's T^2 and SPE statistics, to evaluate their effectiveness in identifying abnormal operating conditions. A multivariate time-series dataset comprising seven different operational scenarios and 18 process variables from the AGRU system was used as input for both models. The overall implementation strategy for the LSTM-AE and PCA approaches is illustrated in Fig. 3.

PCA is a statistical technique capable of handling multiple variables and anomalies that normally occur in industrial data using T^2 and SPE techniques [70]. The original dataset was transformed into principal components (PCs) and undergoes several steps before being projected into the new PCA space. Firstly, the data was scaled, and then its covariance was calculated. In the PCA method, the original data was scaled to a matrix $\boldsymbol{X}$ with zero mean and unit variance. Then, based on a singular value decomposition (SVD) algorithm, the matrix $\boldsymbol{X}$ can be decomposed using the given Eq. (2) [71]:

$$\boldsymbol{X}_{\text{Reconstructed}} = \boldsymbol{T}\boldsymbol{P}^T \tag{2}$$

where $\boldsymbol{T}$ is the score matrix and $\boldsymbol{P}$ is the loading matrix.

The PCA model includes number of PCs, which are calculated by cumulative percent variance (CPV) using the Eq. (2) [72, 73].

$$\text{CPV}_\ell = \frac{\sum_{i=1}^{l} \lambda_i}{\sum_{i=1}^{m} \lambda_l} \tag{3}$$

The PCA transforms the original set of m variables to ℓ PCs where $\boldsymbol{\lambda}$ is the variance of the score vector and m is the total number of variables. The corresponding number of PCs was determined by setting CPV larger than 95%. In PCA-based anomaly detection, control limits and statistics must be identified to check the normal and abnormal behavior of the process [68, 71]. SPE is a commonly used statistical method that indicates deviation in the discarded (residual) space, whereas T^2 indicates sample deviation in the PC space, indicating a potential fault.

The T^2 statistic was calculated by using Eq. (4) [74, 75].

$$T^2 = x^T \boldsymbol{p} \Lambda^{-1} \boldsymbol{p}^T x \tag{4}$$

Where x is the data point and Λ is the eigenvalue. The $\boldsymbol{p}$ contains the eigenvectors. The threshold of T^2 is calculated using the F-distribution method mentioned in Eq. (5).

$$T^2_{\text{lim}} = \frac{\ell(m-1)}{m-l} F_{\ell,m-1,\alpha} \tag{5}$$

Where Fisher distributions are represented by $F_{\ell,m-1,\alpha,\ell}$, and $(m - \ell)$ are the degrees of freedom. Whereas α is the significance level. The SPE was determined as follows [75]:

$$\text{SPE} = \left\| \boldsymbol{x}^T_{\text{new}} - \boldsymbol{x}^T_{\text{new}} \boldsymbol{P}_a \boldsymbol{P}^T \right\|^2 \tag{6}$$

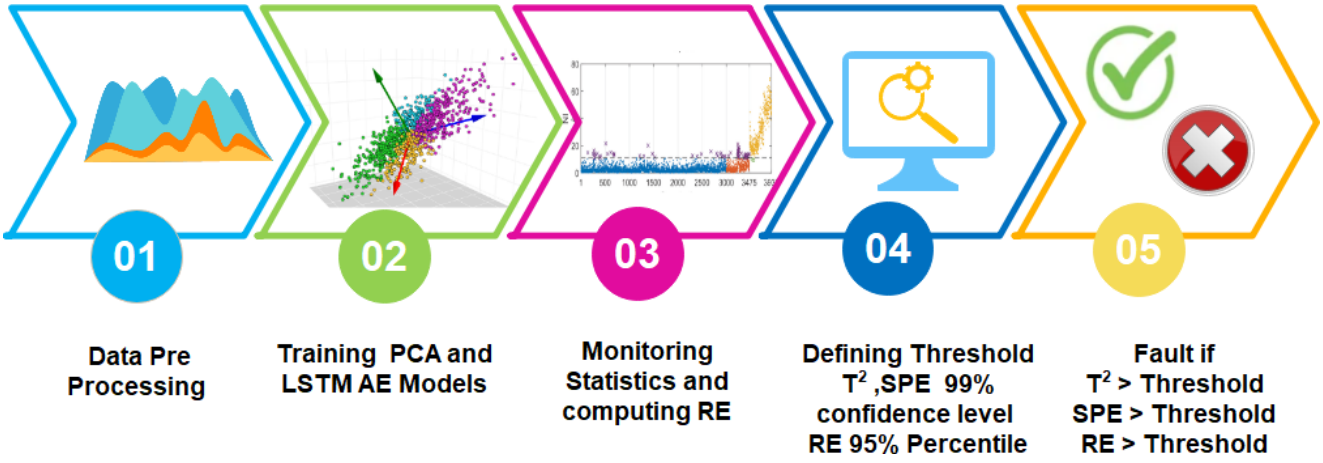

Fig. 3 Sequence of FD model

Where, $\boldsymbol{x}_{\text{new}}$ is an observed vector to be detected. $\boldsymbol{P}_a$ is ($\boldsymbol{m} \times \boldsymbol{a}$) matrix that comprised of the first column of the loading matrix $\boldsymbol{P}$ and $\boldsymbol{P}_a$ is a $\boldsymbol{m} \times (\boldsymbol{m} - \boldsymbol{a})$ matrix that is comprised of the rest of the columns of $\boldsymbol{P}$. The threshold limit was calculated by using Chi-Square approximation as illustrated as Eq. (7) [72].

$$\text{SPE}_{\text{threshold}} = \theta_1 \left[\frac{C_\alpha \sqrt{2\theta_2 h_o^{\,2}}}{\theta_2} + 1 + \frac{\theta_2 h_o \left(h_o - 1\right)}{\theta_2^2} \right]^{\frac{1}{h_o}} \qquad \theta_i = \sum_{j=a+1}^{n} \lambda i \left(i = 1,2,3\right) \quad h_o = 1 - \frac{2\theta_1 \theta_3}{\theta_2^2} \tag{7}$$

The C_α has been taken from the standard classification. The PCA-based model was first developed using data from normal operating conditions. Subsequently, T^2 and SPE-based monitoring control charts were applied to the faulty dataset. An observation was flagged as abnormal when the values of T^2 or SPE exceeded their respective thresholds.

While PCA-based FD provided a useful baseline by highlighting deviations in the latent space, it exhibited limitations in distinguishing between actual faults and transient noise. To enhance robustness, an LSTM-AE model was developed for FD. LSTM-AE was developed to model the normal operating behavior of the system and identify faults based on deviations in RE. The model is trained exclusively on normal (fault-free) data, allowing it to capture the underlying temporal dependencies and variable interactions that characterize healthy system dynamics. Once trained, the model evaluates incoming time-series sequences and compares them to the learned baseline behavior.

Significant deviations in RE are interpreted as indicators of faulty or abnormal conditions. The input dataset, consisting of multivariate time-series measurements, is first normalized to a [0, 1] range using Min-Max scaling to ensure consistent variable scaling across all features. The normalized data is segmented into overlapping sequences of fixed length n. Each sequence served as an input sample to the LSTM-AE. A stacked LSTM-AE was implemented using PyTorch to model normal system behavior and detect deviations based on RE. The model architecture consists of a two-layer LSTM encoder with 128 hidden units per layer, followed by a fully connected layer that compresses the encoded sequence into a 32-dimensional latent representation. The decoder mirrors this structure, using a linear transformation to expand the latent space to 64 dimensions, which is then passed through a two-layer LSTM decoder with 64 units, reconstructing the original input shape.

The model was trained using the Adam optimizer with a learning rate of 0.001, a batch size of 32, and trained over 50 epochs on fault-free data. RE was computed as the mean squared error between the input and output sequences. The model is trained to minimize the mean squared RE between the input and the reconstructed sequence. The RE for a sequence is computed as Eq. (8):

$$\text{RE} = \frac{1}{n \times m} \sum_{i=1}^{n} \sum_{j=1}^{m} \left(x_{t-n+i,j} - x'_{t-n+i,j} \right)^2 . \tag{8}$$

Where x and x' represent the reconstructed values of the j^{th} variable at the i^{th} time step within the sequence. After training, the LSTM-AE is evaluated on the complete dataset, including both normal and potentially faulty regions. For each input sequence, the RE is computed and monitored. A FD threshold δ is determined empirically using Eq. (9) based on the 95$^{\text{th}}$ percentile of the REs obtained from the training data.

$$\delta = \text{Percentile}_{95} \left(\text{RE train} \right) \tag{9}$$

If $\text{RE}_t > \delta$ at time t exceeds this threshold, the corresponding sample is flagged as faulty. This data-driven thresholding approach enables the detection of anomalies without requiring prior knowledge of specific fault patterns. The use of an LSTM-AE empowers the model to capture temporal dependencies in multivariate process data, allowing for early and accurate detection of both abrupt and gradually evolving faults.

5.2 Deep learning multiclass fault diagnosis model

GRU and LSTM are advanced types of RNNs designed to address the vanishing gradient problem and effectively capture long-term dependencies in sequential data. Both models are widely used in time-series analysis, natural language processing, and FD in industrial processes due to their ability to retain relevant information over extended sequences [54, 57, 76, 77].

LSTM consists of three key gates, namely input, forget, and output gates, that regulate the flow of information through a memory cell. This structure enables LSTM to selectively retain important information and discard irrelevant data, making it highly effective for handling long-term dependencies in complex datasets. GRU, on the other hand, is a simplified version of LSTM with only two gates, the update and reset gates. This streamlines its architecture and reduces computational complexity while maintaining performance. Unlike LSTM, GRU has a streamlined structure with fewer gating mechanisms (reset and

update gates), resulting in a reduced number of trainable parameters. This enables faster convergence during training and lower inference latency, key requirements for real-time deployment in industrial settings such as AGRUs. Additionally, GRU's ability to capture essential temporal dependencies without the added complexity of cell states (as in LSTM) contributes to improved generalization with less computational overhead, making it more suitable for edge-based or resource-constrained environments.

In comparison, LSTM is generally preferred when working with long and complex sequences, as it can better preserve information over extended time steps. GRU, being less computationally demanding, is often favored for tasks requiring faster training and inference while still capturing important sequential patterns. Both models have demonstrated strong performance in FDD applications, with LSTM excelling in capturing intricate dependencies and GRU offering a balance between accuracy and efficiency [59, 77].

The architecture of Bi-LSTM and Bi-GRU is shown in Figs. 4 and 5, along with Eqs. (10)–(19), in which z_t is the input gate, r_t is the reset gate, h' is the new hidden state, h is the candidate output of hidden layer, o is the output of GRU, f_t is the forget gate LSTM, i_t is the input gate, c_t is the current cell state, c_t' is the new cell state, h_t is the hidden state.

$$z_t = \sigma_g\left(W_z \times x_t + U_z \times h_{t-1} + b_z\right) \tag{10}$$

$$r_t = \sigma_g\left(W_r \times x_t + U_r \times h_{t-1} + b_r\right) \tag{11}$$

$$h' = \tanh\left(W_h \times x_t + r \times U_h \times h_{t-1} + b_z\right) \tag{12}$$

$$h = \left(z \times h_{t-1}\right) + \left(1 - z\right) \times h' \tag{13}$$

$$o = \sigma_g\left(W_o h_t + b_o\right) \tag{14}$$

$$f_t = \sigma_g\left[\left(W_f \times X_t\right) + \left(U_f \times h_{t-1}\right) + b_f\right] \tag{15}$$

$$i_t = \sigma_g\left[\left(W_o \times X_t\right) + \left(U_o \times h_{t-1}\right) + b_f\right] \tag{16}$$

$$c_t = \left(f_t \times c_{t-1} + i_t \times c_t'\right) \tag{17}$$

$$c_t' = \tanh\left[\left(W_c \times X_t\right) + \left(U_c \times h_{t-1}\right) + b_c\right] \tag{18}$$

$$h_t = o_t \times \tanh\left(c_t\right) \tag{19}$$

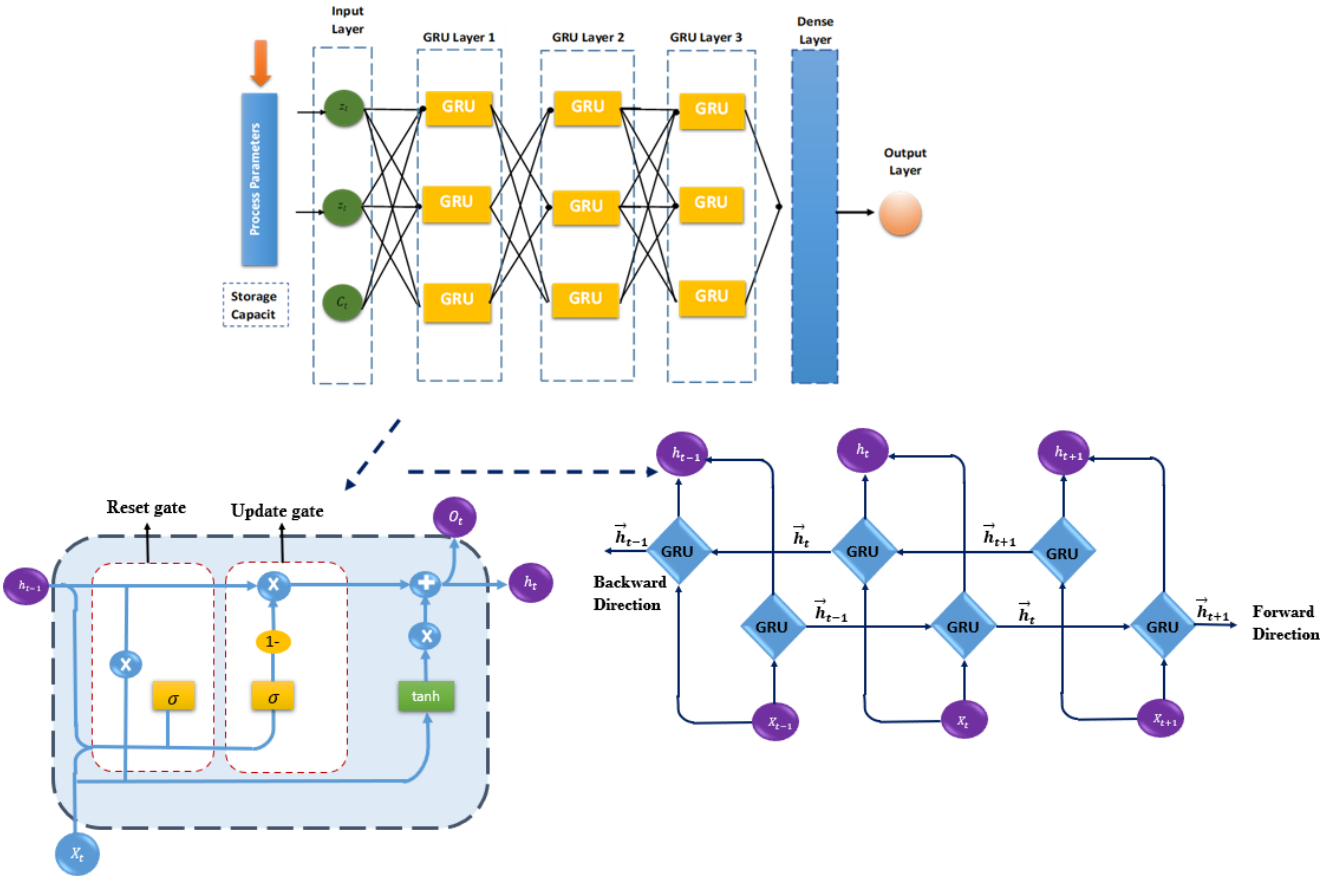

Fig. 4 Architecture of Bi-GRU

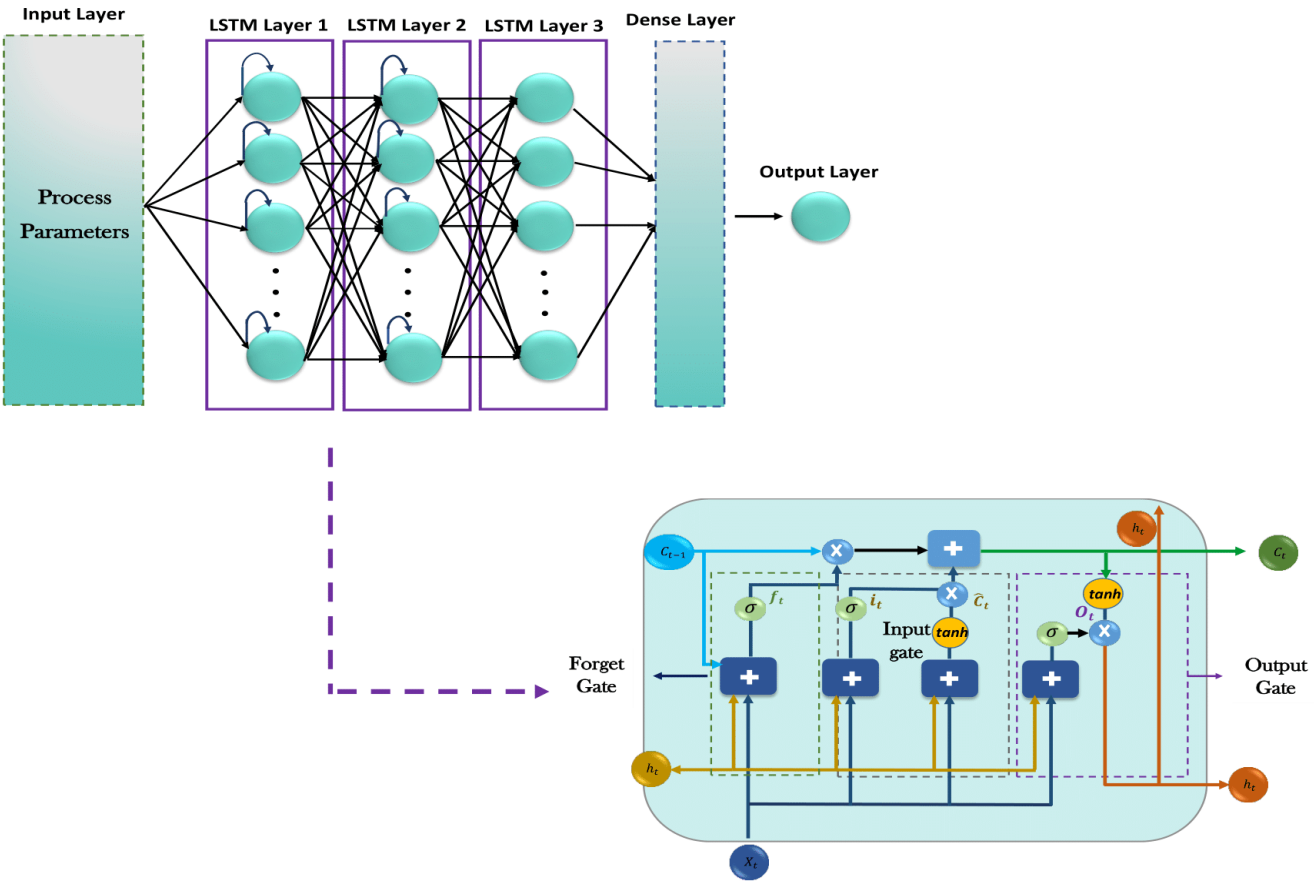

Fig. 5 Architecture of Bi-LSTM

The performance of both models was systematically evaluated in this research, with complete hyperparameter settings provided in Table 5. The multiclass and multivariate classification model was developed using a Python environment, in which the Keras [78] package and TensorFlow [79] were applied for the Bi-GRU and Bi-LSTM networks using 70% as a training set and 15% as a validation and test set using the obtained data. The dataset contains both normal and abnormal data for training.

AGRU data was preprocessed by eliminating the useless or invalid data points from the dataset, and the sliding window method was applied. Then, the input data was loaded into the networks for the diagnosis of fault type. The architecture of the models was finalized using the Keras tuner. A library designed explicitly for hyperparameter tuning in Keras models. Hyperparameter tuning is essential to optimize the performance of Bi-GRU and Bi-LSTM-based models [77] It involves systematically

Table 5 Configuration of hyperparameters for Bi-GRU and Bi-LSTM models

Hyper parameter	GRU model	LSTM model
Layer 1	Bidirectional 128 units	Bidirectional 96 units
Layer 2	128 units	160 units
Layer 3	32 units	64 units
Activation function	tanh	tanh
L2 regularization parameter (with each layer)	0.0067	0.005
Dropout (after each layer)	0.3, 0.2, 0.2	0.1, 0.1, 0.2
Dense layer	64 units with ReLU activation	32 units with ReLU activation
Activation function on output layer	Softmax	Softmax
Optimizer and learning rate	Adam, 0.0003	Adam, 0.0001
Epochs	200	200
Loss function	Categorical cross entropy	Categorical cross entropy

searching for the best combination of hyperparameters to improve the model's accuracy, generalization, and efficiency. *K*-fold cross-validation was used to validate both models. This resampling technique evaluates machine learning models by dividing the dataset into *K* subsets (folds) [6]. The model was trained on *K*-1 folds and tested on the remaining fold, repeating the process 10 times with different test folds.

5.3 Performance assessment of the models

FD methods aim to identify faulty conditions while minimizing false alarms accurately. Key evaluation metrics include fault detection rate (FDR) and false alarm rate (FAR), where FDR measures the model's ability to detect actual faults correctly, and FAR represents the proportion of normal conditions misclassified as faults [6]. The performance of LSTM-AE and PCA-based FD was assessed using FAR and FDR, as defined in Eq. (16) and Eq. (17). To evaluate the effectiveness of the proposed fault diagnosis system using deep learning models (Bi-GRU and Bi-LSTM), performance metrics such as accuracy, precision, recall, and F1-score were utilized. Accuracy represents the overall correctness of the model's predictions, precision quantifies the proportion of true positive (TP) predictions among all predicted positives, recall assesses the model's ability to identify actual positive cases correctly, and the F1-score offers a balanced measure by computing the harmonic mean of precision and recall. These metrics are further detailed in Eqs. (20)–(24).

$$\text{FDR} = \frac{\text{TP}}{\text{TP} + \text{FN}} \tag{20}$$

$$\text{FAR} = \frac{\text{FP}}{\text{FP} + \text{TN}} \tag{21}$$

In Eqs. (17)–(22), TP refers to correctly identified faulty conditions, meaning the model accurately detects an actual fault. True negative (TN) represents correctly classified normal conditions, where no fault is present, and the model correctly identifies it as such. A false positive (FP) occurs when the model incorrectly classifies a normal condition as faulty, leading to a false alarm. False negative (FN) happens when the model fails to detect an actual fault, classifying it as normal instead [6].

$$\text{Accuracy} = \frac{\text{TP} + \text{TN}}{\text{TP} + \text{FP} + \text{TN} + \text{FN}} \tag{22}$$

$$\text{F1 Score} = \frac{2 \times \text{Precision} \times \text{Recall}}{\text{Precision} + \text{Recall}} \tag{23}$$

$$\text{Recall} = \frac{\text{TP}}{\text{TP} + \text{FN}} \tag{24}$$

$$\text{Precision} = \frac{\text{TP}}{\text{TP} + \text{FP}} \tag{25}$$

6 Results and discussion

Section 6 presents three critical aspects of fault analysis in the AGRU system. First, it examines the system's behavior in response to various faults, offering insights into how process variables deviate under abnormal conditions. Second, it focuses on FD using analytical approaches that identify deviations from normal operation. Ultimately, the study employs a deep learning algorithm to address fault diagnosis, utilizing advanced predictive modeling techniques to accurately classify faults and identify their root causes.

6.1 Behavior of AGRU

Section 6.1 presents the behavior of the absorption column under fault conditions. In the Supplement, Fig. S1 illustrates the process under normal operating conditions, while Figs. S2–S7 depict various fault scenarios. Faults 1 and 2 are associated with cooler fouling and an increase in sour gas temperature, respectively. These faults were introduced by applying step changes to the cooler duty and gas temperature, as shown in Figs. S2 and S3. Once each set point was reached, the subsequent fault condition was introduced into the system. Both faults disrupted the temperature profile within the column. In particular, the sour gas temperature increased from 35 °C to 55 °C, significantly reducing the absorption efficiency and compromising the quality of the sweet gas. As a result, the CO_2 concentration in the treated gas increased to 0.019 mol/mol. It was also observed that higher sour gas temperatures elevated the temperatures of the sweet gas and rich amine streams. To mitigate these effects, the lean amine feed must be supplied at a lower temperature, and additional cooling may be required to reduce the temperature of the recycled amine below that of the fresh amine feed. A standard operational practice is to maintain a temperature difference of more than 5 °C between the rich amine feed and the sour gas feed to ensure efficient gas absorption. A reduction in this temperature difference can lead to foaming, which negatively impacts tray hydraulics and destabilizes the liquid level at the bottom of the column.

Fault 3 was introduced as a step change in the sour gas flow rate, as shown in Fig. S4. The sour gas flow was initially increased to 9000 kmol/h, followed by small step increases and decreases to observe the system's response. This change can induce entrainment flooding, which reduces the liquid-to-vapor (L/V) ratio in the column, ultimately degrading the quality of the sweet gas stream due to elevated CO_2 composition.

In typical AGRU design and operation, feedback control is commonly employed to regulate the CO_2 concentration in the outlet sweet gas (the controlled variable) by adjusting the inlet amine flow rate (the manipulated variable). This control relationship is reflected in the corresponding response of the amine flow rate. Additionally, a high sour gas flow rate can entrain the MDEA solution, causing upward liquid carryover and leading to downcomer flooding. This flooding increases the liquid level on the trays and at the bottom of the column, as observed in the simulation results, which negatively affects separation efficiency and allows the CO_2 concentration to exceed 2 mol%. Moreover, the elevated sour gas flow disturbs the sweet gas temperature due to the increased gas volume entering the system.

Fault 4 was simulated by increasing the differential pressure across the column, a condition typically associated with foaming. Foaming is primarily caused by contaminated feed, resulting in abrupt fluctuations in tray levels and bottom levels, as illustrated in Fig. S5. When this fault occurs, the CO_2 removal efficiency declines, as indicated by an increase in the CO_2 concentration in the sweet gas, reaching 0.017 mol/mol. Foaming can result in liquid carryover to subsequent trays and may also lead to stage flooding. This undesirable process condition disrupts both liquid and vapor flow patterns within the column. Such disturbances are evident from the changes observed in the amine flow rate and the bottom liquid level, confirming the negative impact of foaming on column performance and separation efficiency.

Fault 5 was implemented as a step change in the column, simulating a loss of amine flow. This loss disrupts the liquid-to-gas (L/G) ratio, which is critical for maintaining the quality of the sweet gas. As a result, the CO_2 concentration in the sweet gas increases, reaching 0.027 mol/mol, as shown in Fig. S6. The imbalance between liquid and gas flows also causes the sweet gas flow rate to rise to 5100 kmol/h. The reduction in amine flow not only decreases the rich amine stream, but also leads to an overall increase in column temperature due to the higher gas throughput. This temperature rise further impacts the performance of the regenerator and the recycled amine stream, ultimately compromising the system's separation efficiency.

Fault 6 in this study represents tray corrosion resulting from the deposition of contaminants, and it was simulated by reducing tray efficiency, as illustrated in Fig. S7. Corrosion leads to a decrease in active surface area and a loss of contact area, which disrupts the balance between liquid and gas flows. This imbalance reduces contact time, thereby impairing the overall performance of the column. Under normal operating conditions, tray efficiency is maintained at 80%. To simulate the fault condition, the efficiency of multiple trays was reduced to below 5%, which led to a significant increase in CO_2 concentration at the column top and a reduction in the pressure of the sweet gas stream, indicating a pressure drop within the column. As observed in the system responses, this pressure drop negatively impacted tray levels and also influenced the rich amine flow rate at the column bottom, further deteriorating the column's separation efficiency.

6.2 Fault detection

The LSTM-AE demonstrates effective FD across six distinct fault cases (F_1–F_6), as illustrated in the RE plots in Fig. 6 (a)–(f). Each plot highlights the RE (black line), the detection threshold (red dashed line), and the faulty regions (red shaded areas), where the error exceeds the threshold. The shaded regions visually represent the periods during which the model detects faults. The performance evaluation of the LSTM-AE and PCA-based FD method is assessed using the FDR and FAR, as presented in Table 6.

In all cases, the model accurately identifies these periods, as reflected by the FDR values. Specifically, F_6 achieves an FDR of 1.00, indicating complete detection of the injected faults, and FDR for remaining faults F_1–F_5 lie in the range of 0.9–0.99, which also shows good detection. The corresponding FARs are extremely low (ranging from 0.001 to 0.003), showing that the AE rarely misclassifies normal data as faulty. Based on the detection outcomes presented in Fig. 6 for fault 1, it is evident that the LSTM-AE is highly reliable in distinguishing between normal and faulty conditions. The absence of false alarms (FAR = 0.000) demonstrates that the model is trained exclusively on normal (fault-free) data, enabling it to learn the underlying dynamics of the normal process with high fidelity. As a result, the RE for unseen normal sequences remains consistently below the decision threshold, ensuring that no normal samples are incorrectly flagged as faults. However, some faults

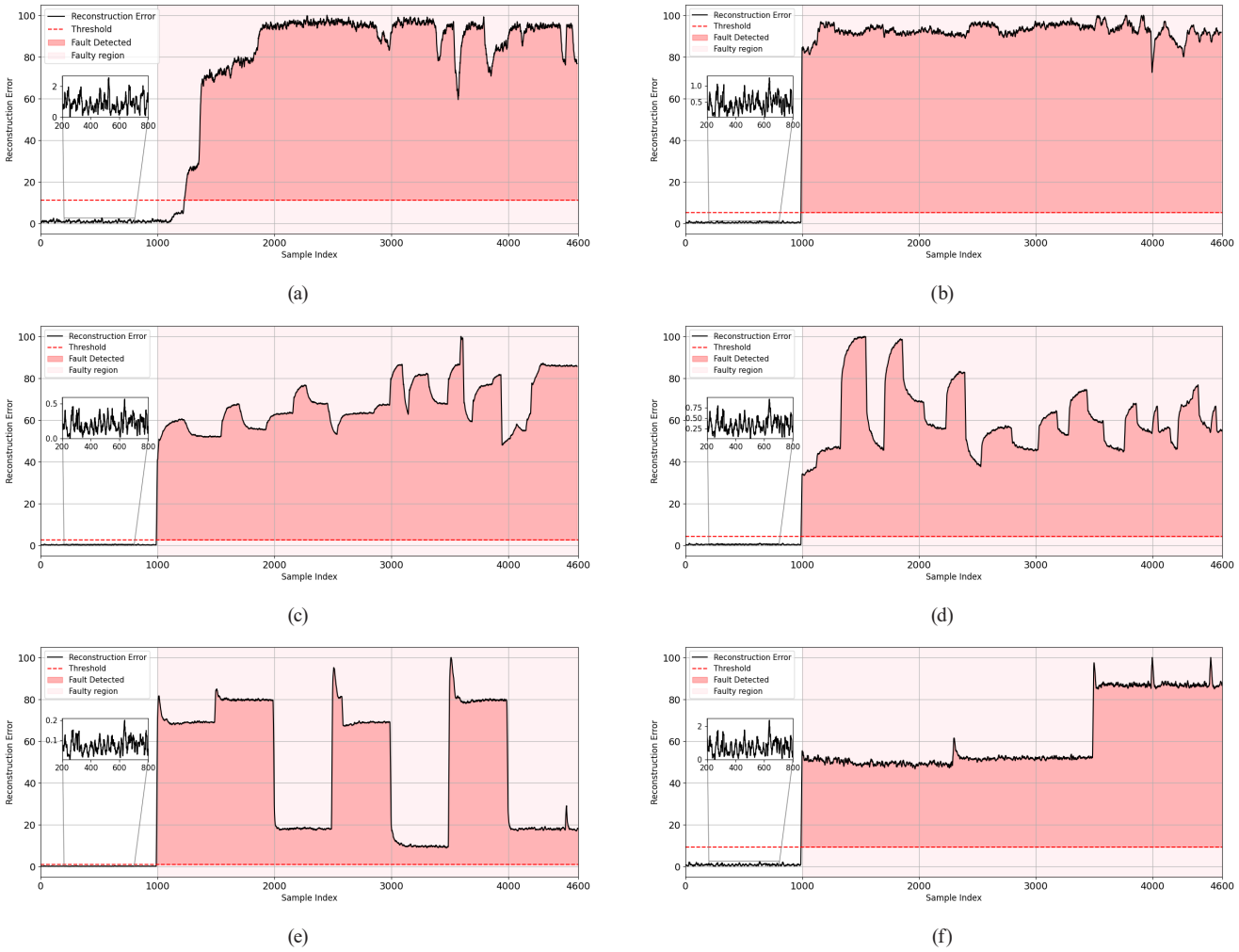

Fig. 6 RE plot for LSTM-AE (a) Fault 1: cooler fouling (b) Fault 2: high sour gas temperature (c) Fault 3: high sour gas flow (d) Fault 4: increase in differential pressure (e) Fault 5: loss of amine flow (f) Fault 6: damaged tray

Table 6 Performance evaluation of PCA and LSTM-AE models

Fault	LSTM-AE FDR	LSTM-AE FAR	PCA T^2 FDR	PCA T^2 FAR	PCA SPE FDR	PCA SPE FAR
F_1	0.93	0.00	0.812	0.06	0.810	0.055
F_2	0.99	0.003	0.82	0.03	0.814	0.02
F_3	0.96	0.0018	0.875	0.03	0.879	0.03
F_4	0.95	0.0012	0.838	0.020	0.834	0.015
F_5	0.949	0.002	0.78	0.02	0.79	0.06
F_6	1.00	0.001	0.878	0.03	0.88	0.03

are incorrectly flagged as normal and remain undetected. These undetected cases (FN = 228) may correspond to fault transitions or low-magnitude fault manifestations where the RE did not significantly exceed the decision threshold. The FDR of 0.935 suggests that the model successfully detected the majority of faults, with only a small proportion (6.5%) of fault samples remaining undetected. This reflects the model's ability to distinguish between genuine faults and natural process variability, thereby avoiding spurious alarms and ensuring strong robustness during normal operations, which is a critical requirement for industrial FD systems. Unnecessary alarms can lead to operational inefficiencies. For fault F_2, illustrated in Fig. 7 (b), the LSTM-AE achieved an almost perfect FDR = 0.99 with a minimal FAR = 0.003, indicating its capability to identify even subtle deviations from normal operation. Likewise, for faults F_3, F_4, and F_5, the LSTM-AE consistently yielded high detection rates (0.949–0.96) with very low false alarms (all ≤ 0.002), confirming the model's robustness in generalizing across diverse fault types while avoiding misclassification of normal data as faulty. Overall, the LSTM-AE–based detector demonstrates a favorable balance between achieving a high FDR and maintaining zero false alarms, making it particularly suitable for deployment in safety-critical applications where false alarms can be costly. The correspondence between elevated REs and the onset of fault

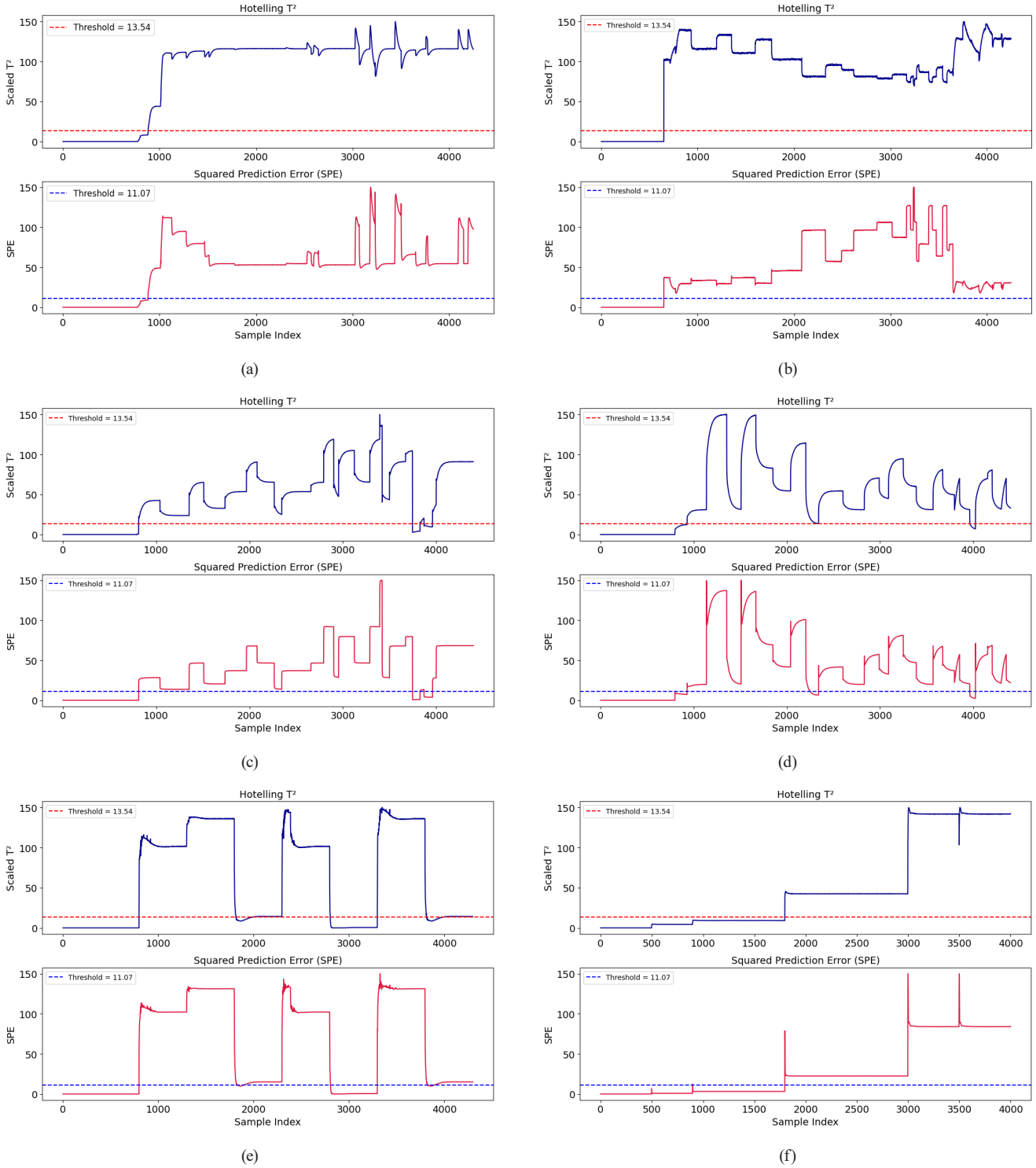

Fig. 7 T^2 and SPE for process faults (a) Fault 1: cooler fouling (b) Fault 2: high sour gas temperature (c) Fault 3: high sour gas flow (d) Fault 4: increase in differential pressure (e) Fault 5: loss of amine flow (f) Fault 6: damaged tray

conditions indicates that the model is capable of capturing both abrupt and gradual deviations from normal operation. Moreover, the consistently low FARs confirm that these detections are not attributable to noise or normal variability, thereby underscoring the robustness and reliability of the proposed approach for FD in time series data.

In addition to the deep learning-based approach, the T^2 statistic evaluates how well a sample conforms to the PCA-defined latent space by capturing variations along the PCs. In contrast, the SPE statistic measures deviations in the residual space, representing variance not explained by the PCs. The plots of T^2 and SPE for faults are shown

in Fig. 7 (a)–(f). The 95% T^2 threshold limit is shown with a red dotted line, and the 95% SPE threshold is set to capture 95% of the normal process variability. Samples lie below the threshold, indicating that the process is operating within normal limits. Samples exceed the threshold, signaling a deviation from normal operating conditions. The results of fault 1 are illustrated in Fig. 7 (a), which indicates that the model correctly identified 3476 fault samples as TPs. In comparison, 774 fault samples are misclassified as normal FNs. In terms of normal data, 1000 samples are correctly classified as TNs, whereas 47 normal samples are incorrectly flagged as faulty FPs. Based on these outcomes, FDR achieved a value of 0.818, indicating that approximately 81.8% of faults were successfully detected and FAR is found to be 0.06, corresponding to only 6% of normal samples being incorrectly flagged as faults. Approximately similar results are observed from SPE. The comparative analysis of the T^2 and SPE–based PCA FD indices highlights both similarities and subtle differences in their performance across the six fault scenarios.

The comparative analysis between the LSTM-AE and PCA-based FD methods as presented in Table 6, highlights the clear superiority of the deep learning approach. The comparison clearly highlights the limitations of linear methods against advanced deep learning models. PCA, being a linear dimensionality reduction technique, assumes that process variations can be adequately explained by a small number of orthogonal PCs. While this works reasonably well for simple linear correlations, it struggles to capture the nonlinear dynamics and temporal dependencies that are common in industrial processes. As a result, the FDR values for PCA (T^2: 0.78–0.88, SPE: 0.79–0.88) remain consistently lower than those of the LSTM-AE (0.93–1.00). Moreover, PCA's SPE and projection-space monitoring (T^2) are both sensitive to process noise and minor normal fluctuations, which explains the relatively high FARs of 0.015–0.06. In contrast, the LSTM-AE achieves FARs close to zero (0.00–0.003) because it learns temporal patterns and nonlinear mappings directly from normal operating data. By reconstructing sequences rather than isolated snapshots, the LSTM-AE can distinguish between genuine faults and harmless variations, leading to much more reliable monitoring performance.

Therefore, the superior results of the LSTM-AE can be attributed to its ability to handle nonlinear, time-dependent process behaviors, whereas PCA's reliance on linear projections makes it less effective for complex FD tasks. This explains why PCA tends to miss certain faults or raise unnecessary alarms, while the LSTM-AE provides both higher sensitivity and robustness in practical applications.

6.3 Performance assessment of DL models

The outcomes of the evaluated models are tabulated in Table 7. Model performance was evaluated using standard classification metrics, including accuracy, precision, recall, and F1 score. Among all models, the Bi-GRU exhibited the best overall performance. Its architecture, which dynamically retains past information through a simplified gating mechanism without the use of a separate cell state, makes it particularly robust to noisy inputs and less prone to overfitting short-term fluctuations. The GRU achieved an accuracy of 99.8%, successfully identifying all six faults present in the AGRU system test samples. Its high precision of 99.8% indicates minimal FPs, while a recall of 99.7% confirms that it successfully captured nearly all true fault events. The F1 score of 99.7% further demonstrates its balanced and reliable classification capability.

In terms of computational efficiency, GRU also outperformed LSTM, due to its simpler structure. The Bi-GRU trained and predicted faster than the Bi-LSTM, making it a more practical choice for real-time FD scenarios where low latency is critical. Nonetheless, LSTM may still be preferred in applications that benefit from its greater modeling capacity, albeit at the cost of longer processing times. While both deep learning models demonstrated excellent performance, their suitability for deployment depends not only on accuracy but also on execution speed and resource availability.

In addition to LSTM and GRU, classical machine learning models, namely random forest (RF), XGBoost, logistic regression, and *K*-nearest neighbors (KNN), were evaluated for comparison, illustrated as Table 8. Although these models achieved reasonably high accuracies (97.5% for XGBoost, 98.8% for RF, 96.3% for logistic regression, and 98.4% for KNN), they consistently underperformed relative to the deep learning approaches. Moreover, their lower recall and F1 scores indicate a reduced capacity to detect subtle or sequential fault patterns. Unlike GRU and

Table 7 Performance evaluation of models

Model	Accuracy	Precision	Recall	F1 score	Average training time/epoch	Average prediction time/epoch
Bi-GRU	99.8%	0.998	0.997	0.997	0.012 s	0.002 s
Bi-LSTM	99.1%	0.990	0.991	0.990	0.06 s	0.008 s

Table 8 Performance comparison of fault diagnosis models

Model	Accuracy (%)	Precision	Recall	F1 score
XGBoost	97.5	0.965	0.965	0.967
RF	98.8	0.978	0.98	0.98
KNN	98.4	0.984	0.983	0.983
Logistic regression	96.3	0.97	0.96	0.96

LSTM, these traditional models are limited in their ability to model temporal dependencies, which are critical in FD for dynamic, multivariate processes such as AGRU systems. This comparison further highlights the superior ability of GRU and LSTM models to capture time-dependent fault behavior effectively.

The proposed models were also benchmarked against the work of Kathlyn et al. [57], who conducted a classification study on AGRU FD. The proposed GRU and LSTM architectures achieved accuracies of 99.8% and 99.1%, respectively, outperforming the shallow sparse autoencoder without tuning (89.47%), with tuning (99.39%), and the deep sparse autoencoder without tuning (90.73%). Although the fine-tuned deep sparse autoencoder achieved a comparable accuracy of 99.9%, the proposed models offer competitive performance with only a marginal difference. This improvement can be attributed to the optimized architecture of the proposed models, which effectively captures the complex nonlinear relationships within the AGRU process data. Additionally, the use of more robust regularization and hyperparameter optimization strategies contributed to better generalization and reduced overfitting compared to conventional sparse autoencoder configurations.

6.4 Quantitative analysis

The conventional method of the confusion matrix is used for the quantitative analysis of the diagnostic results of AGRU. The outcomes of these models are illustrated in Figs. 8 and 9. The rows and columns of the confusion matrix represent the predicted faults and the true faults, respectively. The match between the predicted and true faults is indicated by a diagonal, while the errors of the tested algorithm are displayed in off-diagonal cells. According to the confusion matrix of the GRU, the accuracy of fault 5 is 95%, and the remaining faults are classified with 99% accuracy in the GRU model. The confusion matrix of the Bi-LSTM model indicates that it performs well in predicting the correct faults. However, fault 2 has a small error rate of 0.02, meaning that 2% of instances are misclassified, and fault 5 has a 16% misclassification rate, suggesting that the model struggles slightly with

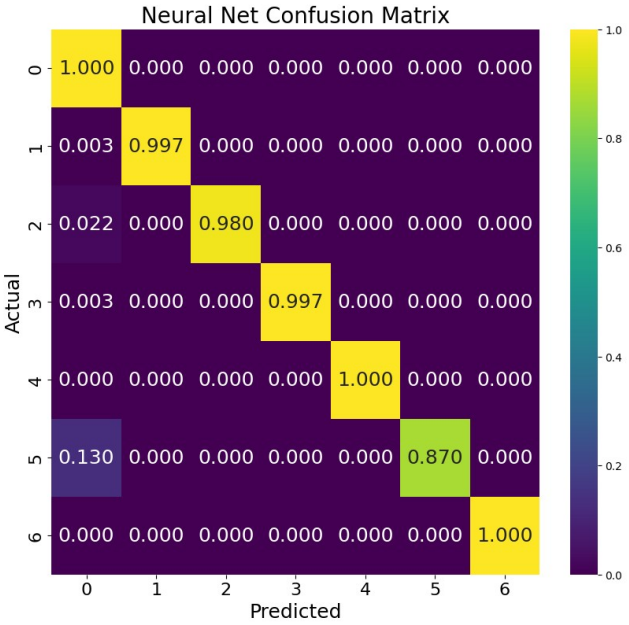

Fig. 8 Confusion matrix of GRU

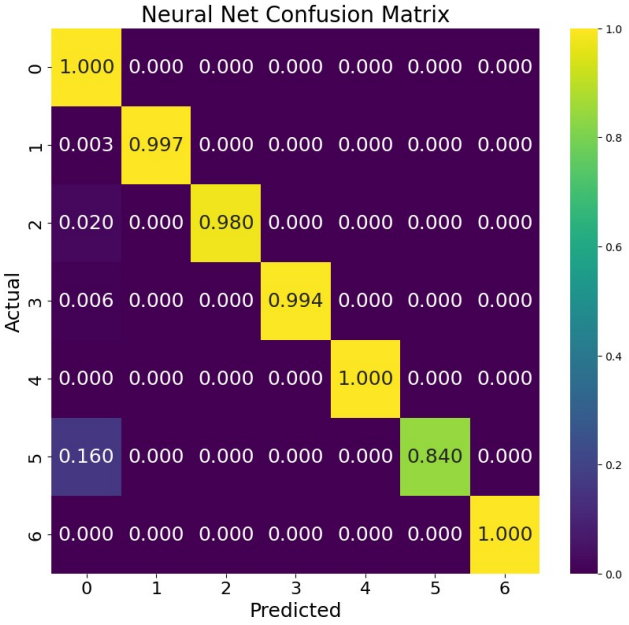

Fig. 9 Confusion matrix of LSTM

distinguishing these two faults. Other faults have a nearly perfect classification (value ≈ 1.0).

6.5 SHAP analysis

Explainable AI refers to techniques and tools that help make the decisions and predictions of machine learning models understandable to humans [80]. SHAP is a method that provides a way to interpret complex models by assigning a value to each feature, representing its contribution to the model's prediction. This makes it easier to understand which features are driving the model's decisions and

how they interact with each other. SHAP is a key tool in the field of Explainable AI, due to its superior capacity to reveal both individual feature contributions and pairwise interaction effects within complex industrial processes. By using SHAP, data scientists and researchers can gain insights into the model's behavior, making it more transparent and trustworthy. Fig. 10 is a heat map depicting the fault-wise SHAP interaction. The SHAP-based fault analysis provides clear correspondence between variable importance and underlying physical mechanisms across the six studied fault scenarios. For cooler fouling (F_1), heat-transfer inefficiency elevates the importance of amine temperature (x_4) and sour-gas flow (x_3), with downstream flow variables (x_9, x_{12}) also becoming influential, while tray levels remain relatively uninformative. In the case of high sour-gas temperature (F_2), sour-gas temperature (x_2) emerges as the most dominant factor, accompanied by sweet-gas temperature (x_8), while pressure and flow variables show moderate contributions and level variables are negligible. High gas flow (F_3) is primarily characterized by sour-gas and sweet-gas flows (x_3, x_9), supported by pressure indicators (x_7, x_{10}), whereas temperature variables play a minor role. High differential pressure (F_4) is best explained by rich-amine pressure (x_{10}), with sweet-gas pressure (x_7) and sweet-gas flow (x_9) also exhibiting strong contributions; in contrast, temperatures and liquid levels remain of low

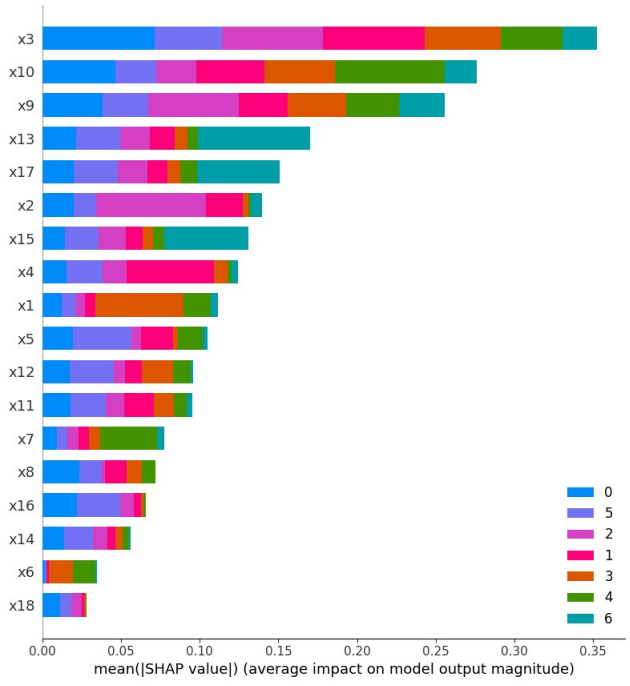

Fig. 10 SHAP model explanation

importance. For loss of amine flow (F_5), stage liquid levels (x_{16}) and circulation flows (x_5, x_{12}) dominate the SHAP profile, while sour-gas temperature (x_2) shows a moderate effect and other pressure and level measurements are secondary. Finally, damaged tray faults (F_6) are strongly associated with tray-level variables (x_{13}, x_{15}, x_{17}), with sour-gas flow (x_3) contributing modestly and temperature and pressure variables showing reduced influence.

Overall, the results indicate that temperature-driven faults (F_1, F_2) elevate the importance of temperature and flow variables, flow-driven faults (F_3, F_5) emphasize flow and level measurements, and hydraulic or flooding-related faults (F_4, F_6) are best captured by pressure and level indicators. This consistency between SHAP importance and the physical mechanisms of fault propagation reinforces the interpretability of the model and highlights its potential to guide targeted sensor selection for early FD in the gas sweetening process.

To demonstrate the real-time applicability of the proposed FDD framework, its deployment potential in industrial environments, such as PLCs and DCS, is carefully considered. Once trained offline, the LSTM-AE and GRU models can be efficiently deployed using lightweight inference engines (e.g., TensorFlow Lite or ONNX), enabling FD to be refreshed every few seconds in accordance with the process data sampling rate. Integration with existing plant infrastructure can be achieved via standard industrial communication protocols such as OPC-UA or Modbus, using a sliding time window (e.g., 30–60 s) for continuous anomaly detection. The framework is robust against transient conditions, start-up sequences, load changes, and fault progression, as demonstrated through dynamic simulation data reflecting real-world operating scenarios.

In conclusion, the fusion of deep learning with SHAP-driven interpretability not only demystifies the model's decision-making process but also enhances its readiness for real-time deployment in safety-critical AGRU operations. By delivering accurate, transparent, and actionable insights into fault origins, the proposed framework advances the safe and efficient monitoring of complex chemical process units. While SHAP's theoretical soundness justified its application in this study, alternative methods like LIME offer scalability advantages for real-time use. Future work could explore hybrid strategies such as using LIME for rapid fault screening and SHAP for detailed root cause analysis or assess newer explainability techniques tailored for industrial time-series data.

7 Conclusion

In this study, a hybrid framework was proposed for multiclass FDD in an AGRU dynamic system. PCA was employed for initial FD using Hotelling's T^2 and SPE statistics, effectively capturing deviations in process variables with a FDR exceeding 95%. However, the PCA-based method exhibited high variability in T^2 and transient spikes, leading to false alarms in certain scenarios. In contrast, the LSTM-AE demonstrated superior robustness and interpretability in detecting faults, particularly under dynamic conditions. Its ability to model temporal dependencies reduced false alarms and eliminated the need for manual threshold tuning, making it a more reliable option for real-time monitoring.

For fault diagnosis, deep learning models, specifically LSTM and GRU networks, were utilized to classify faults based on temporal patterns in multivariate time-series data. Among these, the GRU model outperformed, achieving an overall accuracy of 99.8% and an F1-score of 99.6%, ensuring precise classification across all fault scenarios. To enhance model transparency, an explainable AI technique, including SHAP was integrated. SHAP analysis revealed that the most highly influential variables across all fault types are sour-gas temperature (x_2), amine temperature (x_4), sour-gas flow (x_3), sweet-gas flow (x_9), rich-amine pressure (x_{10}), and tray liquid levels (x_{13}–x_{17}). These variables represent the most sensitive indicators of abnormal behavior in the sweetening process and provide strong candidates for prioritization in sensor selection and monitoring. These findings underscore the effectiveness of combining statistical process monitoring with deep learning and explainability techniques for robust and interpretable FDD in complex industrial environments. Future work will involve incorporating noisy field-acquired data, applying robust denoising techniques, and developing adaptive learning mechanisms. Additionally, real-time integration of the proposed framework into live AGRU systems will be explored to evaluate its performance under varying operational loads and transient conditions. The Future work will focus on incorporating field-acquired noisy data, robust denoising methods, and adaptive learning mechanisms, integrating this model into live AGRU systems and evaluating its performance under varying operating loads and transient states.

Acknowledgement

The authors would like to acknowledge the support given by the Department of Polymer and Petrochemical Engineering, NED University of Engineering and Technology. This work was funded by the Ministry of Science and Technology (MoST) Endowment Fund, Government of Pakistan.

Declaration of competing interest

The authors declare that they have no known competing financial interests or personal relationships that could have appeared to influence the work reported in this article.

References

[1] Lee, J., Cameron, I., Hassall, M. "Improving process safety: What roles for Digitalization and Industry 4.0?", Process Safety and Environmental Protection, 132, pp. 325–339, 2019. https://doi.org/10.1016/j.psep.2019.10.021

[2] Liu, S., Liu, Q., Ahmed, S., Wang, J., Lei, F., Zhao, D. "A method for the early prediction of abnormal conditions in chemical processes combined with physical knowledge and the data-driven model", Journal of Loss Prevention in the Process Industries, 86, 105185, 2023. https://doi.org/10.1016/j.jlp.2023.105185

[3] Ababneh, H., AlNouss, A., Karimi, I. A., Al-Muhtaseb, S. A. "Natural Gas Sweetening Using an Energy-Efficient, State-of-the-Art, Solid–Vapor Separation Process", Energies, 15(14), 5286, 2022. https://doi.org/10.3390/en15145286

[4] Taqvi, S. A., Tufa, L. D., Zabiri, H., Maulud, A. S., Uddin, F. "Multiple Fault Diagnosis in Distillation Column Using Multikernel Support Vector Machine", Industrial & Engineering Chemistry Research, 57(43), pp. 14689–14706, 2018. https://doi.org/10.1021/acs.iecr.8b03360

[5] Taqvi, S. A. A., Zabiri, H., Tufa, L. D., Uddin, F., S. A. Fatima, Maulud, A. S. "A Review on Data-Driven Learning Approaches for Fault Detection and Diagnosis in Chemical Processes", ChemBioEng Reviews, 8(3), pp. 239–259, 2021. https://doi.org/10.1002/cben.202000027

[6] Taqvi, S. A. A., Zabiri, H., Uddin, F., Naqvi, M., Tufa, L. D., Kazmi, M., Rubab, S., Naqvi, S. R., Maulud, A. S. "Simultaneous fault diagnosis based on multiple kernel support vector machine in nonlinear dynamic distillation column", Energy Science & Engineering, 10(3), pp. 814–839, 2022. https://doi.org/10.1002/ese3.1058

[7] Kamil, M. Z., Khan, F., Halim, S. Z., Amyotte, P., Ahmed, S. "A methodical approach for knowledge-based fire and explosion accident likelihood analysis", Process Safety and Environmental Protection, 170, pp. 339–355, 2023. https://doi.org/10.1016/j.psep.2022.11.074

[8] Arunthavanathan, R., Khan, F., Ahmed, S., Imtiaz, S. "Remaining Useful Life Estimation Using Fault to Failure Transformation in Process Systems", IEEE Systems Journal, 17(2), pp. 2512–2522, 2023. https://doi.org/10.1109/JSYST.2022.3205179

[9] Cen, J., Chen, H., Wu, Y., Si, W., Zhao, B., Yang, Z., Tang, L., Liu, S. "Robust fault detection for chemical processes based on dynamic low-rank matrix and optimized LSTM", Process Safety and Environmental Protection, 178, pp. 18–33, 2023. https://doi.org/10.1016/j.psep.2023.07.094

[10] Kaib, M. T. H., Kouadri, A., Harkat, M. F., Bensmail, A., Mansouri, M. "Improving kernel PCA-based algorithm for fault detection in nonlinear industrial process through fractal dimension", Process Safety and Environmental Protection, 179, pp. 525–536, 2023. https://doi.org/10.1016/j.psep.2023.09.010

[11] Liu, N., Hu, M., Wang, J., Ren, Y., Tian, W. "Fault detection and diagnosis using Bayesian network model combining mechanism correlation analysis and process data: Application to unmonitored root cause variables type faults", Process Safety and Environmental Protection, 164, pp. 15–29, 2022. https://doi.org/10.1016/j.psep.2022.05.073

[12] Alauddin, M., Khan, F., Imtiaz, S., Ahmed, S., Amyotte, P. "Integrating process dynamics in data-driven models of chemical processing systems", Process Safety and Environmental Protection, 174, pp. 158–168, 2023. https://doi.org/10.1016/j.psep.2023.04.008

[13] Feng, Z., Li, Y., Xiao, B., Sun, B., Yang, C. "Process monitoring of abnormal working conditions in the zinc roasting process with an ALD-based LOF-PCA method", Process Safety and Environmental Protection, 161, pp. 640–650, 2022. https://doi.org/10.1016/j.psep.2022.03.064

[14] Amin, M. T., Khan, F., Ahmed, S., Imtiaz, S. "A data-driven Bayesian network learning method for process fault diagnosis", Process Safety and Environmental Protection, 150, pp. 110–122, 2021. https://doi.org/10.1016/j.psep.2021.04.004

[15] Hu, J., Zhang, L., Cai, Z., Wang, Y., Wang, A. "Fault propagation behavior study and root cause reasoning with dynamic Bayesian network based framework", Process Safety and Environmental Protection, 97, pp. 25–36, 2015. https://doi.org/10.1016/j.psep.2015.02.003

[16] Alauddin, M., Khan, F., Imtiaz, S., Ahmed, S., Amyotte, P. "A robust neural network model for fault detection in the presence of mislabelled data", The Canadian Journal of Chemical Engineering, 102(4), pp. 1368–1380, 2024. https://doi.org/10.1002/cjce.25181

[17] Pang, C., Duan, D., Zhou, Z., Han, S., Yao, L., Zheng, C., Yang, J., Gao, X. "An integrated LSTM-AM and SPRT method for fault early detection of forced-oxidation system in wet flue gas desulfurization", Process Safety and Environmental Protection, 160, pp. 242–254, 2022. https://doi.org/10.1016/j.psep.2022.01.062

[18] Tao, Q., Xin, B., Zhang, Y., Jin, H., Li, Q., Dai, Z., Dai, Y. "A novel triage-based fault diagnosis method for chemical process", Process Safety and Environmental Protection, 183, pp. 1102–1116, 2024. https://doi.org/10.1016/j.psep.2024.01.072

[19] Khan, N., Taqvi, S. A. A. "2 - Natural gas sweetening standards, policies, and regulations", In: Advances in Natural Gas: Formation, Processing, and Applications. Volume 2: Natural Gas Sweetening, Elsevier, 2024, pp. 33–53. ISBN 978-0-443-19217-3 https://doi.org/10.1016/B978-0-443-19217-3.00019-2

[20] Moghadasi, M., Ozgoli, H. A., Farhani, F. "A machine learning-based operational control framework for reducing energy consumption of an amine-based gas sweetening process", International Journal of Energy Research, 45(1), pp. 1055–1068, 2021. https://doi.org/10.1002/er.6159

[21] Kohl, A. L., Nielsen, R. "Gas Purification", Elsevier, 1997. ISBN 9780884152200

[22] Hakimi, M., Omar, M. B., Ibrahim, R. "Application of Neural Network in Predicting H2S from an Acid Gas Removal Unit (AGRU) with Different Compositions of Solvents", Sensors, 23(2), 1020, 2023. https://doi.org/10.3390/s23021020

[23] Khan, N., Taqvi, S. A. A. "3 - Economic assessments and environmental challenges of natural gas sweetening technologies", In: Advances in Natural Gas: Formation, Processing, and Applications. Volume 2: Natural Gas Sweetening, Elsevier, 2024, pp. 55–72. ISBN 978-0-443-19217-3 https://doi.org/10.1016/B978-0-443-19217-3.00009-X

[24] El-Bagoury, M., Shaker, I., Yaser, S., Hamdy, O., Emad, H., Nassar, M., Abouseada, N., Bassyouni, M. "Environmental analysis of Acid Gas Sweetening with DEA", International Journal of Industry and Sustainable Development, 5(2), pp. 47–72, 2024. https://doi.org/10.21608/ijisd.2024.297793.1056

[25] Amiri, N., Benyounes, H., Lounis, Z., Shen, W. "Design of absorption process for CO_2 capture using cyano based anion ionic liquid", Chemical Engineering Research and Design, 169, pp. 239–249, 2021. https://doi.org/10.1016/j.cherd.2021.03.014

[26] Taqvi, S. A. A., Zabiri, H., Singh, S. K. M., Tufa, L. D., Naqvi, M. "Investigation of control performance on an absorption/stripping system to remove CO_2 achieving clean energy systems", Fuel, 347, 128394, 2023. https://doi.org/10.1016/j.fuel.2023.128394

[27] Tikadar, D., Gujarathi, A. M., Guria, C. "Towards retrofitting based multi-criteria analysis of an industrial gas sweetening process: Further insights of CO_2 emissions", Process Safety and Environmental Protection, 175, pp. 259–271, 2023. https://doi.org/10.1016/j.psep.2023.05.011

[28] Salvinder, K. M. S., Zabiri, H., Taqvi, S. A., Ramasamy, M., Isa, F., Rozali, N. E. M., Suleman, H., Maulud, A., Shariff, A. M. "An overview on control strategies for CO_2 capture using absorption/stripping system", Chemical Engineering Research and Design, 147, pp. 319–337, 2019. https://doi.org/10.1016/j.cherd.2019.04.034

[29] Verma, N., Verma, A. "Amine system problems arising from heat stable salts and solutions to improve system performance", Fuel Processing Technology, 90(4), pp. 483–489, 2009. https://doi.org/10.1016/j.fuproc.2009.02.002

[30] AbuKashabeh, A., Pal, P., Al-Asheh, S., Banat, F. "Formation of heat stable salts during thermal degradation of aqueous methyldiethanolamine (MDEA) solvent and corrosion studies with different alloys", International Journal of Current Research, 6(5), pp. 6582–6587, 2014. [online] Available at: https://www.journalcra.com/article/formation-heat-stable-salts-during-thermal-degradation-aqueous-methyldiethanolamine-mdea [Accessed: 09 March 2025]

[31] Bi, X., Qin, R., Wu, D., Zheng, S., Zhao, J. "One step forward for smart chemical process fault detection and diagnosis", Computers & Chemical Engineering, 164, 107884, 2022. https://doi.org/10.1016/j.compchemeng.2022.107884

[32] Askarian, M., Benítez, R., Graells, M., Zarghami, R. "Data-based fault detection in chemical processes: Managing records with operator intervention and uncertain labels", Expert Systems with Applications, 63, pp. 35–48, 2016. https://doi.org/10.1016/j.eswa.2016.06.040

[33] Taqvi, S. A. A., Kumar, K., Malik, S., Zabiri, H., Ahmad, F. "Prediction of heat exchanger fouling for predictive maintenance using artificial neural networks", Chemical Papers, 78(15), pp. 8295–8308, 2024. https://doi.org/10.1007/s11696-024-03668-z

[34] Ha, D., Ahmed, U., Pyun, H., Lee, C.-J., Baek, K. H., Han, C. "Multi-mode operation of principal component analysis with k-nearest neighbor algorithm to monitor compressors for liquefied natural gas mixed refrigerant processes", Computers & Chemical Engineering, 106, pp. 96–105, 2017. https://doi.org/10.1016/j.compchemeng.2017.05.029

[35] Kumar, A., Bhattacharya, A., Flores-Cerrillo, J. "Data-driven process monitoring and fault analysis of reformer units in hydrogen plants: Industrial application and perspectives", Computers & Chemical Engineering, 136, 106756, 2020. https://doi.org/10.1016/j.compchemeng.2020.106756

[36] Madakyaru, M., Harrou, F., Sun, Y. "Monitoring Distillation Column Systems Using Improved Nonlinear Partial Least Squares-Based Strategies", IEEE Sensors Journal, 19(23), pp. 11697–11705, 2019. https://doi.org/10.1109/JSEN.2019.2936520

[37] Pradittiamphon, S., Wongsa, S. "Fault detection and isolation of acid gas removal units in a gas separation process using PLS", In: 2016 International Conference on Instrumentation, Control and Automation (ICA), Bandung, Indonesia, 2016, pp. 88–93. ISBN 978-1-5090-1336-4 https://doi.org/10.1109/ICA.2016.7811481

[38] Al-Sinbol, G., Perhinschi, M. G. "Development of an Artificial Immune System for Power Plant Abnormal Condition Detection, Identification, and Evaluation", International Review of Automatic Control (IREACO), 10(3), pp. 218–228, 2017. https://doi.org/10.15866/ireaco.v10i3.11739

[39] Cheng, H., Liu, Y., Huang, D., Cai, B., Wang, Q. "Rebooting kernel CCA method for nonlinear quality-relevant fault detection in process industries", Process Safety and Environmental Protection, 149, pp. 619–630, 2021. https://doi.org/10.1016/j.psep.2021.03.025

[40] Dai, Y., Cheng, F., Wu, H., Wu, D., Zhao, J. "Chapter Five - Data driven methods", In: Methods in Chemical Process Safety, vol. 4, Elsevier, 2020, pp. 167–203. ISBN 78-0-12-821824-2 https://doi.org/10.1016/bs.mcps.2020.02.002

[41] Deng, X., Wu, M., Yang, W., Tang, X., Cao, Y. "Fault detection of multimode chemical processes using weighted density peak clustering and trend slow feature analysis", Process Safety and Environmental Protection, 196, 106941, 2025. https://doi.org/10.1016/j.psep.2025.106941

[42] Qin, R., Lv, F., Ye, H., Zhao, J. "Unsupervised transfer learning for fault diagnosis across similar chemical processes", Process Safety and Environmental Protection, 190, pp. 1011–1027, 2024. https://doi.org/10.1016/j.psep.2024.06.060

[43] Shahid, M., Zabiri, H., Taqvi, S. A. A., Hai, M. "Fault root cause analysis using degree of change and mean variable threshold limit in non-linear dynamic distillation column", Process Safety and Environmental Protection, 189, pp. 856–866, 2024. https://doi.org/10.1016/j.psep.2024.07.001

[44] Figueroa Barraza, J., Guarda Bräuning, L., Benites Perez, R., Morais, C. B., Martins, M. R., Droguett, E. L. "Deep learning health state prognostics of physical assets in the Oil and Gas industry", Proceedings of the Institution of Mechanical Engineers, Part O: Journal of Risk and Reliability, 236(4), pp. 598–616, 2022. https://doi.org/10.1177/1748006X20976817

[45] Han, S., Yang, L., Duan, D., Yao, L., Gao, K., Zhang, Q., …, Gao, X. "A novel fault detection and identification method for complex chemical processes based on OSCAE and CNN", Process Safety and Environmental Protection, 190, pp. 322–334, 2024. https://doi.org/10.1016/j.psep.2024.08.055

[46] Chen, Y., Zhang, C., Zhang, R., Gao, F. "Deep network model fusion of wide kernel feature learning for industrial process modeling and fault diagnosis", Process Safety and Environmental Protection, 194, pp. 1283–1302, 2025. https://doi.org/10.1016/j.psep.2024.12.066

[47] Honti, B., Farkas, A., Nagy, Z. K., Pataki, H., Nagy, B. "Explainable deep recurrent neural networks for the batch analysis of a pharmaceutical tableting process in the spirit of Pharma 4.0", International Journal of Pharmaceutics, 662, 124509, 2024. https://doi.org/10.1016/j.ijpharm.2024.124509

[48] Bao, Y., Wang, B., Guo, P., Wang, J. "Chemical process fault diagnosis based on a combined deep learning method", The Canadian Journal of Chemical Engineering, 100(1), pp. 54–66, 2022. https://doi.org/10.1002/cjce.24153

[49] Yu, J., Yan, X. "A new deep model based on the stacked autoencoder with intensified iterative learning style for industrial fault detection", Process Safety and Environmental Protection, 153, pp. 47–59, 2021. https://doi.org/10.1016/j.psep.2021.07.002

[50] Khan, N., Ammar Taqvi, S. A. "Machine Learning an Intelligent Approach in Process Industries: A Perspective and Overview", ChemBioEng Reviews, 10(2), pp. 195–221, 2023. https://doi.org/10.1002/cben.202200030

[51] Wu, H., Zhao, J. "Deep convolutional neural network model based chemical process fault diagnosis", Computers & Chemical Engineering, 115, pp. 185–197, 2018. https://doi.org/10.1016/j.compchemeng.2018.04.009

[52] Kozlenko, M., Zamikhovska, O., Tkachuk, V., Zamikhovskyi, L. "Deep Learning Based Fault Detection of Natural Gas Pumping Unit", In: 2021 IEEE 12th International Conference on Electronics and Information Technologies (ELIT), Lviv, Ukraine, 2021, pp. 71–75. ISBN 978-1-6654-4297-8 https://doi.org/10.1109/ELIT53502.2021.9501066

[53] Verma, R., Yerolla, R., Besta, C. S. "Deep Learning-based Fault Detection in the Tennessee Eastman Process", In: 2022 Second International Conference on Artificial Intelligence and Smart Energy (ICAIS), Coimbatore, India, 2022, pp. 228–233. ISBN 978-1-6654-0053-4 https://doi.org/10.1109/ICAIS53314.2022.9743021

[54] Lv, F., Wen, C., Bao, Z., Liu, M. "Fault diagnosis based on deep learning", In: 2016 American Control Conference (ACC), Boston, MA, USA, 2016, pp. 6851–6856. ISBN 978-1-4673-8683-8 https://doi.org/10.1109/ACC.2016.7526751

[55] Wang, Y., Pan, Z., Yuan, X., Yang, C., Gui, W. "A novel deep learning based fault diagnosis approach for chemical process with extended deep belief network", ISA Transactions, 96, pp. 457–467, 2020. https://doi.org/10.1016/j.isatra.2019.07.001

[56] Wang, N., Yang, F., Zhang, R., Gao, F. "Intelligent Fault Diagnosis for Chemical Processes Using Deep Learning Multimodel Fusion", IEEE Transactions on Cybernetics, 52(7), pp. 7121–7135, 2022. https://doi.org/10.1109/TCYB.2020.3038832

[57] Kathlyn, T. K., Zabiri, H., Aldrich, C., Liu, X., Mohd Amiruddin, A. A. A. "Fault Detection and Identification in an Acid Gas Removal Unit Using Deep Autoencoders", ACS Omega, 8(22), pp. 19273–19286, 2023. https://doi.org/10.1021/acsomega.2c08109

[58] Xavier, G. M., de Seixas, J. M. "Fault Detection and Diagnosis in a Chemical Process using Long Short-Term Memory Recurrent Neural Network", In: 2018 International Joint Conference on Neural Networks (IJCNN), Rio de Janeiro, Brazil, 2018, pp. 1–8. ISBN 978-1-5090-6015-3 https://doi.org/10.1109/IJCNN.2018.8489385

[59] Zeng, L., Jin, Q., Lin, Z., Zheng, C., Wu, Y., Wu, X., Gao, X. "Dual-attention LSTM autoencoder for fault detection in industrial complex dynamic processes", Process Safety and Environmental Protection, 185, pp. 1145–1159, 2024. https://doi.org/10.1016/j.psep.2024.02.042

[60] Ding, S., Zhu, L., Xu, X. "A Novel LSTM-1DCNN-based Deep Network for Fault Diagnosis in Chemical Process", In: 2022 China Automation Congress (CAC), Xiamen, China, 2022, pp. 3744–3749. ISBN 978-1-6654-6534-2 https://doi.org/10.1109/CAC57257.2022.10055667

[61] Tremblay, D., Watanasiri, S., Song, Y., Chen, C.-C. "Benefits of multi-solvent NRTL models in Aspen Plus®: Best in Class Electrolyte Thermodynamics", Aspen Technology, Burlington, MA, USA, 11-1226-0312, 2012.

[62] Kister, H. Z. "What Caused Tower Malfunctions in the Last 50 Years?", Chemical Engineering Research and Design, 81(1), pp. 5–26, 2003. https://doi.org/10.1205/026387603321158159

[63] le Grange, P., Sheilan, M., Spooner, B. "Why Amine Systems Fail – An in-depth Study of Amine System Failures", 2020. [online] Available at: https://www.researchgate.net/publication/343878839_Trends_in_Tragedy_-_An_in-depth_Study_of_Amine_System_Failures [Accessed: 11 March 2025]

[64] Bennett, B., Lager, A., Potter, D. K., Buckman, J. O., Larter, S. R. "Petroleum geochemical proxies for reservoir engineering parameters", Journal of Petroleum Science and Engineering, 58(3–4), pp. 355–366, 2007. https://doi.org/10.1016/j.petrol.2006.06.009

[65] Kister, H. Z. "Distillation Design", McGraw Hill, 1992. ISBN 9780070349094

[66] Al Mehairbi, M. J., Al Mahri, S. A., Dadach, Z. E. "Simulation of Stripper Flooding Due to the Increase of Feed Flowrate", World Journal of Engineering and Technology, 8(3), pp. 443–455, 2020. https://doi.org/10.4236/wjet.2020.83033

[67] Liu, Y., Wu, D., Chen, M., Zhang, B., Chen, J., Liu, Y. "Identification of Methyldiethanolamine Degradation Products and Their Influence on Foaming Properties during the Desulfurization Process for High-Sulfurous Natural Gas", Industrial & Engineering Chemistry Research, 54(21), pp. 5836–5841, 2015. https://doi.org/10.1021/ie504432d

[68] Ali, H., Maulud, A. S., Zabiri, H., Nawaz, M., Suleman, H., Taqvi, S. A. A. "Multiscale Principal Component Analysis-Signed Directed Graph Based Process Monitoring and Fault Diagnosis", ACS Omega, 7(11), pp. 9496–9512, 2022. https://doi.org/10.1021/acsomega.1c06839

[69] Su, X., Zhang, H., Zhang, J., Long, C., Li, X., Gao, Y., Li, S. "Kernel-PCA-based single-phase earth fault detection model using multilayer perceptron in deep learning", IET Generation, Transmission & Distribution, 18(4), pp. 834–843, 2024. https://doi.org/10.1049/gtd2.13117

[70] Xiao, B., Li, Y., Sun, B., Yang, C., Huang, K., Zhu, H. "Decentralized PCA modeling based on relevance and redundancy variable selection and its application to large-scale dynamic process monitoring", Process Safety and Environmental Protection, 151, pp. 85–100, 2021. https://doi.org/10.1016/j.psep.2021.04.043

[71] Zhu, J., Ge, Z., Song, Z. "Distributed Parallel PCA for Modeling and Monitoring of Large-Scale Plant-Wide Processes With Big Data", IEEE Transactions on Industrial Informatics, 13(4), pp. 1877–1885, 2017. https://doi.org/10.1109/TII.2017.2658732

[72] Zhou, J., Guo, A., Celler, B., Su, S. "Fault detection and identification spanning multiple processes by integrating PCA with neural network", Applied Soft Computing, 14, pp. 4–11, 2014. https://doi.org/10.1016/j.asoc.2013.09.024

[73] Josse, J., Husson, F. "Selecting the number of components in principal component analysis using cross-validation approximations", Computational Statistics & Data Analysis, 56(6), pp. 1869–1879, 2012. https://doi.org/10.1016/j.csda.2011.11.012

[74] Sheriff, M. Z., Botre, C., Mansouri, M., Nounou, H., Nounou, M., Karim, M. N. "Process Monitoring Using Data-Based Fault Detection Techniques: Comparative Studies", In: Demetgul, M., Ünal, M. (eds.) Fault Diagnosis and Detection, InTech, 2017. ISBN 978-953-51-3203-5 https://doi.org/10.5772/67347

[75] Wu, F., Yin, S., Karimi, H. R. "Fault Detection and Diagnosis in Process Data Using Support Vector Machines", Journal of Applied Mathematics, 2014, 732104, 2014. https://doi.org/10.1155/2014/732104

[76] Mirzaei, S., Kang, J.-L., Chu, K.-Y. "A comparative study on long short-term memory and gated recurrent unit neural networks in fault diagnosis for chemical processes using visualization", Journal of the Taiwan Institute of Chemical Engineers, 130, 104028, 2022. https://doi.org/10.1016/j.jtice.2021.08.016

[77] Chollet, F. "Deep learning with Python", Manning, 2017. ISBN 9781617294433

[78] Chollet, F. "Deep learning with Python", Manning, 2021. ISBN 9781638350095

[79] Abadi, M., Barham, P., Chen, J., Chen, Z., Davis, A., Dean, J., …, Zheng, X. "TensorFlow: A System for Large-Scale Machine Learning", In: Proceedings of the 12th USENIX Symposium on Operating Systems Design and Implementation (OSDI '16), Savannah, GA, USA, 2016, pp. 265–283. ISBN 978-1-931971-33-1 [online] Available at: https://www.usenix.org/conference/osdi16/technical-sessions/presentation/abadi [Accessed: 11 March 2025]

[80] Ali, S., Abuhmed, T., El-Sappagh, S., Muhammad, K., Alonso-Moral, J. M., Confalonieri, R., Guidotti, R., Del Ser, J., Díaz-Rodríguez, N., Herrera, F. "Explainable Artificial Intelligence (XAI): What we know and what is left to attain Trustworthy Artificial Intelligence", Information Fusion, 99, 101805, 2023. https://doi.org/10.1016/j.inffus.2023.101805